Investigating Quinone Function in Bacterial Photosynthetic Reaction Centers

by

XINYU ZHANG

A dissertation submitted to the Graduate Faculty in Physics in partial fulfillment of the requirements for the degree of Doctor of Philosophy, The City University of New York

2006

UMI Number: 3231999

ProQuest Information and Learning Company
300 North Zeeb Road
P.O. Box 1346
Ann Arbor, MI 48106-1346

This manuscript has been read and accepted for the

Graduate Faculty in Physics in satisfaction of the

dissertation requirement for the degree of Doctor of Philosophy.

Marilyn R. Gunner

Date

Chair of Examining Committee

Sultan Catto

Date

Executive Officer

Timothy Boyer

Ranajeet Ghose

Ronald Koder

Ruth E. Stark

Supervisory Committee

THE CITY UNIVERSITY OF NEW YORK

Abstract

Investigating Quinone Function in Bacteria Photosynthetic Reaction Centers

by

Xinyu Zhang

Adviser: Professor Marilyn R. Gunner

Bacterial Reaction Centers (RCs) Functions and electron transfer kinetics were measured with the different non-native quinone at the Q_A and Q_B sites. A new low potential quinone 2-methyl,3-dimethylamino-1,4-Naphthoquinone (dMA-NQ) has been synthesized. The quinone was added as a low potential electron donor in the RCs and transfer electron to 1,4-Naphthoquinone (NQ) at Q_B while increasing driving force between Q_A and Q_B sites. The kinetics between those non-native quinones is detectable and characterized. The quinone binding affinity at Q_B site may be 10-20 times weaker than those at Q_A site up to the size of 2-methyl-1,4-Naphthoquinone. The temperature dependence of the back reaction with dMA-NQ as Q_A and NQ as Q_B, the upper level for the energy of NQ_B is estimated.

ACKNOWLEDGEMENTS

I own special gratitude to my thesis advisor Dr. Marilyn R. Gunner for her constant education, guidance, encouragement and support; for giving me an opportunity to work in the field of photosynthesis that I like so much.

I am grateful to thank for Dr. Mahesh Lakshman at City College who help us with quinone synthesis. I want to thank Dr. Jennifer Madeo for helpful discussion. We also thank Dr. Philip Laible for providing bacteria and help in their cultivation sample.

I would like to thank members of my examine committee: Prof. Timothy Boyer, Ronald Koder, Ranajeet Ghose and Ruth E. Stark for all their time and advice.

I would like to thank Hongfeng Du for his help on electronic devices; Sue Turner, Aiping Gao, and Joan Meekins for their kindly assistance and support over the years.

I would like to thank my parents and my family for their support, encouragement and guidance throughout my life.

I would like to thank my parents-in-law for helping me to take care of my daughter Sheryl.

Lastly, I would like to thank my husband, Dr. Hongjie Liu, for all his patience, support and guidance, without which I would not have come this far.

Table of Contents

List of Figures

Introduction

Photosynthesis is the most important biological process on earth. It takes place in plants, algae and a variety of bacteria, converting sunlight to chemical energy. In green plant photosynthesis, carbon dioxide and water are used to synthesize carbohydrates and producing molecular oxygen as a side product.

$$CO_2 + H_2O \xrightarrow{h\nu} CH_2O + O_2$$

These carbohydrates are used as an energy source in plants and animals, finally degraded to carbon dioxide and water in the cell by respiration. Photosynthesis and respiration both carry out the transfer of electrons between donor and acceptor molecules bound in proteins embedded in biological membranes. The biological membranes are sheet-like structures. It composed of lipids with embedded proteins that surround the cells and their internal organelles. The photosynthetic reactions in green plants take place in the chloroplasts, membrane-enclosed organelles. The chloroplast has three membranes: inner, outer and thylakoid. There are three compartments: stroma, thylakoid space and inter-membrane space. Chlorophyll is a photosynthetic pigment found in most plants, algae, and cyanobacteria. Chlorophyll absorbs most strongly in the blue and red but poorly in the green portions of the optical spectrum, Therefore the chlorophyll-containing tissues like plant leaves appears green. The photosynthetic bacteria does not have chloroplasts (or any membrane-bound organelles). Bacterial photosynthesis takes place in the cell membrane. Bacteriochlorophylls which are related to chlrorophylls are photosynthetic pigments that occur in various bacteria. The bacterial photosynthesis does not produce oxygen (Peter Raven. 1999).

The first step is to capture light energy with absorption of a photon by bacteriochlorophyll in all types of photosynthesis,. Bacteriochlorophyll is a porphyrin ring with an Mg^{2+} ion coordinated in the center. Resonance energy transfer allows one pigment to become excited by light and transfer energy between them. The photons can be absorbed by the antenna complexes and be transferred to a special complex known as reaction centers (RCs). RCs is a membrane-bound protein-pigment complex. There is a special pair of chlorophyll molecules (P) that is the only pigment that can be oxidized after excitation by light energy. In the reaction center, the light energy initiates electron transfer between bound co-factors.

The photosynthetic reaction centers (RCs) are classified according to the identity of terminal electron acceptors (Figure 1.3) (Blankenship 1992; Allen, Williams et al. 1998; Heathcote 2002). All type I reaction center have four-Fe -four-sulfur clusters (Fe_4S_4) (Fe-S type) as electron acceptors. This type of reaction centers includes PSI reaction centers of green plants, heliobacteria and green sulfur bacteria. They produce a strong reductant and reduce NAD(P)H directly. The other is type II (pheophytin-quinone type), including PSII in green plants, green filamentous bacteria and purple bacteria (Heathcote 2002). Type I and Type II reaction centers both have quinone as electron acceptors, but type II reaction centers can not reduce $NAD(P)^+$ directly without reverse electron flow. Quinones serve important functions in the energy conserving electron transfer reactions. In each type of reaction centers, the electron transfer sequence generates a reduced state of quinone. In type I photosystem, the secondary electron acceptor is an iron-sulfur complex (Fe_4S_4) that continues the sequence of single electron

acceptors. In type II photosystem, the secondary electron acceptor is another quinone Q_B. In bacterial reaction centers such as the *Rb. Sphaeroides* protein that is the focus of work presented here, both quinones are ubiquinones.

Reaction centers from purple bacteria provide an ideal model for the study of many subjects in chemistry and biology. They are easy to isolate and purify from bacteria and stable in the dark at room temperature (Clayton and Wang 1971). The 3-dimensional crystal structure is available at atomic resolution (Allen, Feher et al. 1987; Allen, Feher et al. 1987; Deisenhofer and Michel 1989; Chang, El-Kabbani et al. 1991; Stowell, McPhillips et al. 1997). The electron transfer pathway has already been elucidated (Feher, Allen et al. 1989; Gunner 1991; Blankenship, Madigan et al. 1995). The electron acceptor Q_A and Q_B are easy to remove from reaction centers, and the native quinone can be replaced by other quinones with different properties to study the kinetics of electron transfer (Okamura, Isaacson et al. 1975; Gunner, Tiede et al. 1982; Woodbury, Parson et al. 1986; Graige, Feher et al. 1998; Li, Takahashi et al. 2000). Many mutants have been made and characterized. Finally, because most of the electron transfer steps in reaction centers occur by quantum tunneling, they function over a wide temperature range, allowing extensive characterization of reaction mechanism (Kleinfeld, Okamura et al. 1984; Gunner, Robertson et al. 1986; Gunner and Dutton 1989; McMahon, Muller et al. 1998).

1.1 Photosynthesis in Plants

Plant photosynthesis occurs in two reactions: water oxidation and carbon dioxide reduction. These two reactions are physically separated. The first water oxidation

reaction is light-dependent. Chlorophyll P680 in PSII and P700 in PSI absorbs light energy and carries out light driven electron transfer. The electrons that were grabbed from water are passed to P700 along a series of molecules in the redox chain, which includes P700 as well as P680, generating NADPH. ATP is formed with using energy stored in the transmembrane proton gradient that is generated at several steps on the electron transfer chain. The light reaction takes place on the thylakoid membrane. The oxygen, a byproduct, passes into the atmosphere through pores in the leaves. The carbon dioxide reduction reaction that takes place in the stroma (outside membrane) is driven by NADPH and ATP generated by the light reaction. In this dark reaction, glucose is generated. Figure 1.1 shows the light dependent reaction pathway in plant photosynthesis. Photosynthesis in plants is non-cyclic because water is consumed as reactant and oxygen is generated as byproduct (Cramer and Knaff 1991).

1.2 The Structure of Reaction Centers from Purple Bacteria

The first bacterial reaction centers were isolated and purified from the cell by R.K. Clayton and colleagues in the 1960s (Clayton and Wang 1971). The structure of the type II reaction centers from *Rhodopseudomonas viridis* was solved by the X-ray crystallography in 1984 by Johann Deisenhofer, Robert Huber and Hartmut Michel (Deisenhofer, Epp et al. 1984; Deisenhofer, Epp et al. 1985; Deisenhofer and Michel 1989). This was the first 3-dimensional crystal structure of a hydrophobic, integral membrane protein at atomic resolution. Shortly afterwards, the structure of reaction centers from *Rhodobacter Sphaeroides* was solved (Figure 1.2) (Chang, Tiede et al. 1986; Allen, Feher et al. 1987; Allen, Feher et al. 1987; Allen, Feher et al. 1988; Allen, Feher et

al. 1988). Both proteins have the same essential structure except that there is a cytochrome subunit bound in the reaction centers from *Rhodobacter Sphaeroides.*

The *Rhodobacter Sphaeroides* reaction centers structure have 3 polypeptides: L, M and H which have 281, 307, 260 amino acids and molecular weights 28,000, 22,000, and 19,000, respectively (Clayton 1980). Five long hydrophobic helices of L and M subunits span the cell membrane. There are nine cofactors non-covalently bound to the L and M polypeptides. The cofactors are responsible for all the activities in reaction centers such as absorbing light and transferring electron (Figure 1.2). The cofactors are comprised of four bacteriochlorophylls (BChl), two bacteriopheophytins (BPh), two quinones called Q_A and Q_B, and a non-heme iron atom Fe. The cofactors contribute 52% of the total molecular weight (Williams, Steiner et al. 1986). Two of the bacteriochlorophylls (BChl) form a special pair P870 (P for pigments, 870 indicates the wavelength of maximum absorbance change) in van de Waals contact. P870 works as a single electronic unit. One of two remaining bacteriochlorophylls is bound to each subunit ($BChl_L$ and $BChl_M$). Similarly, one bacteriopheophytin is bound to each subunit (H_L and H_M). Q_A is in a loop from the M subunit, and Q_B is mostly surrounded by residues from the L subunit (Figure 1.2). The backbone of subunit L and M and their attached cofactors are arranged in a two-fold symmetry (central local symmetry); the symmetry axis is oriented perpendicular to the membrane plane. The non-heme iron atom Fe is at the symmetry axis between two quinones Q_A and Q_B. The third subunit H with a single membrane-spanning helix is located largely on the cytoplasmic side of the membrane. It breaks the C_2 symmetry.

1.3 Photosynthesis in Bacterial Reaction Centers from *Rb. Sphaeroides*

The initial electron transfer reaction has been well studied in the reaction center of the purple bacteria (Kirmaier and Holten 1987; Feher, Allen et al. 1989; Gunner 1991; Kirmaier and Holten 1993). Photosynthesis in the photosynthetic bacteria takes place in the plasma membrane that is folded into the cell to increase the available surface area. Photosynthesis takes place in the reaction centers embedded in the cell membrane. That energy needed to start photosynthesis can come from direct photon absorption or energy transferred from the light-harvesting complex. The light-harvesting system antenna complexes, include light harvesting complex I and II (LHI and LHII), which collect the light and transfer the excited state energy to reaction centers. When reaction centers are excited by light, the special pair P releases an electron for electron transfer. The electron is transferred from P to H_L (BPh at L branch), Q_A and then to Q_B (Deisenhofer and Michel 1989; Okamoto 1994). At the same time, soluble cytochrome c reduces P^+, replacing the electron that was released from special pair P, permitting a second electron transfer from P to H_L and then to Q_A and Q_B. Q_B receives two electrons and combines with two protons from the internal surface of the membrane to form dihydroquinone Q_BH_2. Q_BH_2 leaves the reaction center moving into the phospholipid bilayer of the cellular membrane. Q_BH_2 then can be re-oxidized and cytochrome c reduced by cytochrome bc1 complex. The reduced cytochrome and oxidized quinone Q_B then return to the reaction center. Finally, the cytochrome bc1 complex releases 4 protons into the external surface of the membrane. So the flow of electrons from Q_BH_2 back to P generates a trans-membrane electrochemical potential gradient of protons. The inside of the cell becomes negatively charged relative to the external medium, and the pH of the

cytosol is higher than the external pH (Zubay 1988).The protons then move back into the cell through an ATPase, and synthesizing ATP (Figure 1.3). It is well established that the in vitro rates of the intra-protein electron transfer reactions and the yields of the various charge-separated intermediates are very similar to those found in vivo.

1.4 Theory of Electron Transfer Reactions

Electron transfer reacting an electron moves from a donor to an acceptor plays important roles in Chemistry and Biology. Fermi's golden rule describes the fundamental equation of non-adiabatic electron transfer:

$$k_{et} = \frac{2\pi}{\hbar} H_{AB}^2 (FC) \qquad (1.1)$$

Where $\hbar$ is Planck's constant; H_{AB}, the electronic interaction matrix which represents the electronic coupling of donor and acceptor states; FC refers to the Frank-Condon weighted density of states. In the non-adiabatic process, the electronic coupling is weak. The integrated overlap of donor and acceptor wavefunctions is:

$$H_{AB}^2 = H_0^2 \exp(-\beta R) \quad (1.2)$$

Where H_0^2 is the maximum electronic coupling, β is the exponential coefficient in units of $Å^{-1}$, R is the distance from center of edge atom of donor to center of edge atom of acceptor.

In non-adiabatic electron transfer processes, the electron tunnels from one quantum state to another. Electron transfer obeys the Frank–Condon principle: electron transfer from one quantum state to another occurs too fast (10^{-15} s) for the nuclear configurations to change. The Frank-Condon factor, FC, is the integrated overlapping the

donor and acceptor nuclear wavefunction of equal energy. It can be expressed in terms of the driving force $-\Delta G^o$ of reaction and the reorganization energy λ. $-\Delta G^o$ is the free energy difference between reactant and product state (Figure 1.4). The reorganization energy λ is defined as the change in free energy that is necessary to distort the equilibrium geometry of reactant to the equilibrium geometry of product without electron transfer. The reorganization energy is related to changes in the bond lengths, bond angles, distance and orientation of the donor, acceptor and the medium. In the simplest model, the nuclei of the acceptor and their surrounding environment are represented by a single simple harmonic oscillator potential representing the reaction coordinate. The electron transfer rate can be expressed as:

$$k_{et} = \frac{2\pi H_{AB}^2 e^{-\beta R}}{\hbar\sqrt{4\pi\lambda k_B T}} \left(\exp[-\frac{(-\Delta G - \lambda)^2}{4\lambda k_B T}] \right) \qquad (1.3)$$

Where k_B is the Boltzman constant, T is temperature. The activation energy E_A is a measure of FC:

$$E_A = \frac{(-\Delta G^o - \lambda)^2}{4\lambda} \qquad (1.4)$$

As the free energy increases, the reaction speed is increased until an optimum free energy is reached. At the optimum energy, $-\Delta G^o = \lambda$, the electron transfer rate k_{et}^o is maximum since the activation energy E_A is equal to zero, the electron transfer reaction is activationless. The maximum electron transfer rate k_{et}^o increases when the temperature decreases (Figure 1.5). The reactant state is thermally distributed to the lower vibration levels. The rate k_{et}^o is approximately the reciprocal of the square root of the temperature ($T^{-1/2}$) (Eqn. 1.3) (Marcus and Sutin 1985; Moser, Keske et al. 1992). Increasing the free

energy, the rate decreases. This region $-\Delta G^o > \lambda$ defined as the Marcus inverted region. (Figure 1.5).

In summary, the electron transfer rate is dependent on:

1). The driving force, $-\Delta G^o$ due to the redox potential difference between electron donor and acceptor;

2). The distance and the relative orientation between donor and acceptor;

3). The relaxation energy associated with the conformational changes that occur with the change of redox state.

1.5 Electron Transfer in the Reaction Center Protein

With a flash of light, an excited singlet state of P* is formed. P* a transient state, decays in 3 ps by charge separation which forms a P^+H^- (P^+BPh^-) state through the transient formation of a $P^+BCh_L^-$ state which decays in 1ps. The charge separation to form $P^+H_L^-$ occurs in 3 ps over a distance of 10.1 Å (edge atom of P to edge atom of H_L). The reaction is unidirectional, with electrons going exclusively down the L branch of reaction centers. The reduced $P^+BCh_M^-$ and $P^+H_M^-$ are not observed. The electron transfer is activationless, with the rate actually increasing 2-3 fold as the temperature is decreased to 5K. The electron returns to the ground state P with a charge recombination half time of ≈ 20 ns (Woodbury, Becker et al. 1985; Martin, Breton et al. 1986); (Shopes and Wraight 1985; Woodbury, Parson et al. 1986) if there is no functional primary electron acceptor Q_A. The $-\Delta G^o$ is approximately 160 meV and $-\Delta G^o \approx \lambda$ for the native reaction centers (Gunner 1991).

In 200ps, the electron moves 10 Å to the first electron acceptor Q_A. More than 98% of reaction centers can absorb a photon and form the $P^+HQ_A^-$ state. The $-\Delta G^o$ is about 670 meV. The electron transfer rate k_{HA} increase 3-4 fold as the temperature decreases from 300K to 5K. In the *Rb. Sphaeroides* reaction centers with native ubiquinone at the Q_A site, the forward electron transfer rate is fastest and $-\Delta G^o \approx \lambda$. In the absence of Q_B and exogenous electron donor to P^+, $P^+Q_A^-$ will decay to the ground state by direct tunneling at a rate k_{AP} over 22.5 Å across the protein. The rate k_{AP} increases from 9 to 37 s^{-1} as the temperature is lowered from room temperature to 5K (Kleinfeld, Okamura et al. 1984; Gunner, Robertson et al. 1986; McMahon, Muller et al. 1998).

From Q_A^-, the electron moves to the secondary electron acceptor Q_B, in 3-200 μs yielding $P^+Q_B^-$. The electron transfers across 14.5 Å. With the native ubiquinone at both Q_A and Q_B site, the $-\Delta G^o_{AB} \approx 60$ meV at pH = 8.

In the absence of the exogenous electron donor cytochrome c, at each stage in the reaction cycle, there are competing charge recombination reactions to transfer the electron back to P^+. The back reaction from Q_A^- or Q_B^- to the ground state P^+ each has two pathways: by the direct tunneling route or by a thermal back reaction (Figure 1.6). For the direct tunneling route, the electrons go back directly to P^+ at the rate k_{AP} or k_{BP} from $P^+Q_A^-$ or $P^+Q_B^-$. For the thermal back reaction, the electrons go back indirectly via a higher energy state at the k_{AHP} or k_{BAP}. The intermediate state is $P^+H^-Q_A$ for $P^+Q_A^-$ or $P^+Q_A^-Q_B$ for $P^+Q_B^-$. The thermal back reaction rate is temperature dependent; the reaction

rates are proportional to the free energy difference between the initial and intermediate states. The relative free energy of different states can be derived and calculated based on the uphill thermal back reaction rate (Woodbury and Allen 1995); (Kleinfeld, Okamura et al. 1984; Mancino, Dean et al. 1984).

1.6 Rationale and Significance

My works focus on the quinone in reaction centers. In reaction centers from *Rhodobacter Sphaeroides*, the same quinone, ubiquinone-10, is found in both Q_A and Q_B quinone sites. However, the Q_A site can be functionally reconstituted with a wide variety of other natural and synthetic quinone substitutes (Baccarini-Melandri, Gabellini et al. 1980; Gunner, Tiede et al. 1982; Gunner, Braun et al. 1985), tightly binding many non-native quinones. However, the secondary quinone-binding site, Q_B site, is generally regarded to be highly specific for its native ubiquinone-10 molecule (Giangiacomo and Dutton 1989). Reconstitution of Q_B function has been successful only with quinones containing the native ubiquinone (UQ) configuration (Baccarini-Melandri, Gabellini et al. 1980; Okamura, Feher et al. 1982; Wraight and Stein 1983). Few of the non-native quinones are functional at the Q_B site. There are two possible reasons that non-native quinones are not functional at the Q_B site: 1) The quinone does not bind to Q_B site. Q_B can occupy at least two different positions (Stowell, McPhillips et al. 1997; Lancaster 1998): one binding site in which the ubiquinone headgroup is proximal to Fe^{2+} atom (inner site). The other binding site in which the ubiquinone headgroup is distal to Fe^{2+} atom (outer site) (Pokkuluri, Laible et al. 2004). The electron transfer from Q_A^- to Q_B occurs only when Q_B is in the proximal position (Stowell, McPhillips et al. 1997). 2) If the quinone can bind at the Q_B site, the free-energy difference $-\Delta G^o$ between the quinone at the

primary quinone-binding site (Q_A) and the secondary quinone-binding site (Q_B) maybe unfavorable so a bound quinone would not be functional at the Q_B site (Giangiacomo and Dutton 1989)

My work replaces the native ubiquinone-10 with a tightly binding and low potential quinone at the Q_A site. Use of lower potential quinones at the Q_A site or higher potential quinones at the Q_B site with can increase the driving force (Giangiacomo and Dutton 1989). Crystal structures with anthraquinone at the Q_A site show that this functional replacement binds in the same location as the native cofactor and does not perturb the protein structure (Kuglstatter, Miksovska et al. 2000). The low potential quinones, which have tight binding affinity at the Q_A site, are used to make forward electron transfer from Q_A^- to Q_B more favorable. With a low potential quinone at the Q_A site, it is possible to place different non-native quinones at the Q_B site to study how the quinone structure influences the binding affinity of quinone, the rate of electron transfer and redox potential level in reaction centers.

1.7 Application

Biological photosynthesis is not a very efficient process for converting energy to chemical energy. Only 1-2% of the solar energy that is absorbed by plants is converted to chemical energy. If the function of photosynthetic reaction centers is better fully understood, perhaps the efficiency could increase. A more efficient photosynthetic process will not only benefit agriculture because the amount of crop can be grown in a shorter time can might but it also help protect the environment. Global warming poses a big challenge for the environment. The increasing amount of carbon dioxide and other

green house gases in the atmosphere increases the average temperature of the atmosphere and oceans. The gases are released by the burning of fossil fuels, land cleaning and agricultures into atmosphere has dramatically increased in recent years. Carbon dioxide is converted to molecular oxygen and glucose in photosynthesis. Therefore, increasing the rate of plant photosynthesis provides a process in which more carbon dioxide can be consumed, a potential solution for global warming and greenhouse effects.

The photosynthesis process can also be applied to electronics, especially for nanotechnology. Photosynthetic reaction centers are a nano-scale molecular diode and photovoltaic devices. With electron transfer as its primary function, the technology could develop to mimic the functional antenna-reaction center complex to power devices, such as laptops and cell phones with photosynthetic reaction centers. A research group in MIT set up one model device. The isolated photosynthetic reaction centers from spinach were placed on the top of a semiconductor layer, one layer of conducting material with gold on the top of the reaction center layer. Once the device was illuminated by laser light, a tiny electronic current was generated. If many reaction centers could work together, enough electronic energy could be generated to power electronics. (Millsaps, Bruce et al. 2001) (Wang, Medforth et al. 2004).

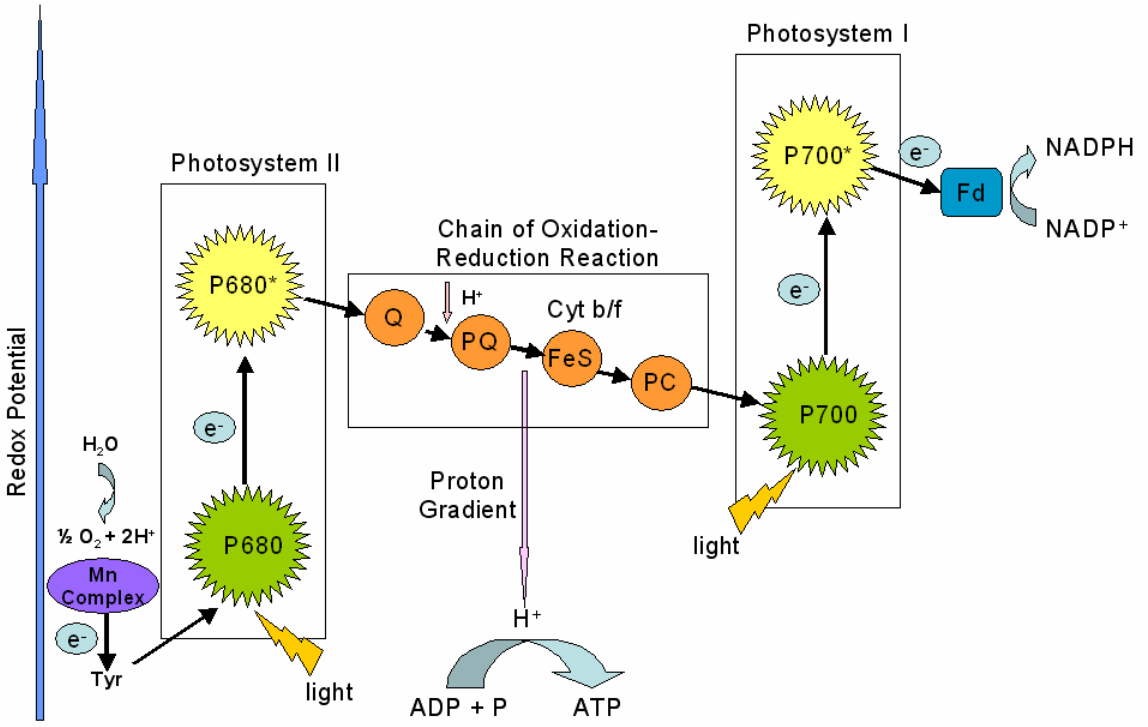

Figure 1.1 The light reaction in plant photosynthesis. The overall reaction is: $2H_2O$ + light energy $\rightarrow$ O_2 + $4H^+$ + 4 electrons. The whole process is known as Non-cyclic Photophosphorylation. Two reaction centers are used: Photosystem II (PSII) and Photosystem I (PSI). PSII is excited by light. P680 then is oxidized and the electron transferred to a quinone. An electron grabbed from the water splitting Mn complex to reduce $P680^+$ reaction that produces molecular oxygen and 4 protons. Four electrons needed to make O_2 from water, thus 4 turnovers are need to oxidize water to O_2. P680 in PSII need to be a strong oxidant to oxidize water and reduce quinone. The electron transfer moves from the quinone through the chain of oxidation-reduction reactions. The cytochrome b/f (Cyt b/f) complex is reduced and pumps protons from the inner membrane to generate the electrochemical proton gradient. The proton gradient can be

employed for the synthesis of ATP. A second, light-activated electron transfer reaction takes place in PSI. PSI is a powerful reductant and that can reduce NADP via ferrodoxin (Fd). The NADPH can be used for reduction of carbon dioxide to glucose in dark the reaction.

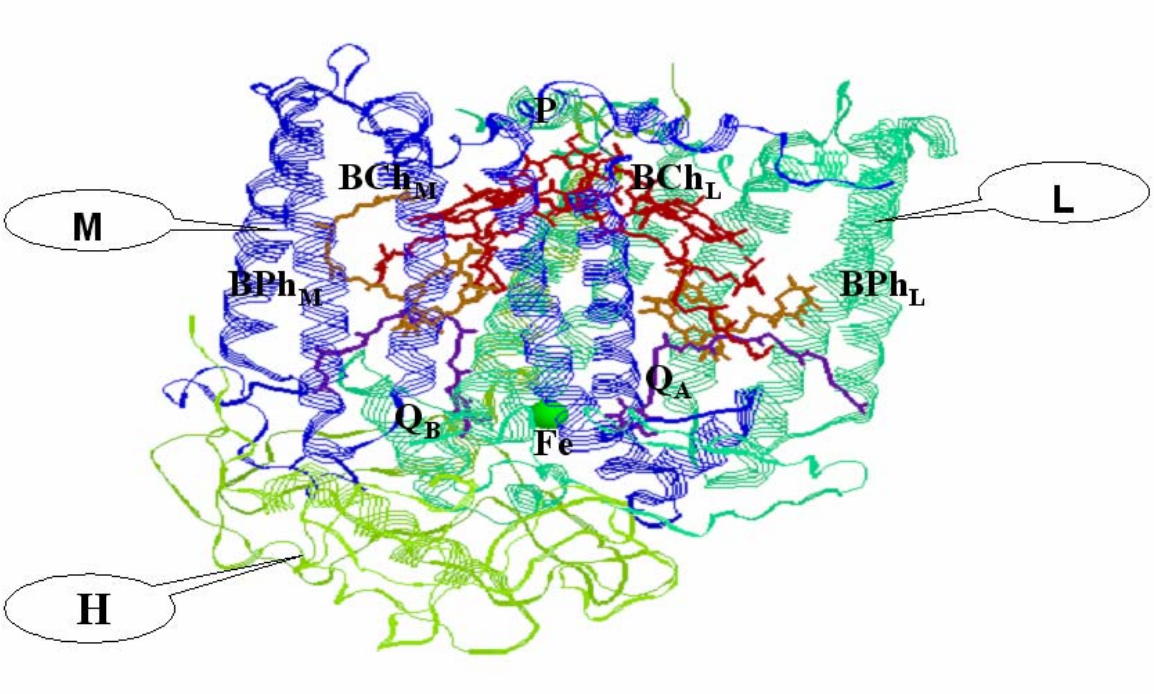

Figure 1.2 Structure of the reaction center protein from the purple bacteria *Rhodobacter sphaeroides*. The complex consists of three protein subunits called M, L, and H. The cofactors are bound to the L and M subunits.

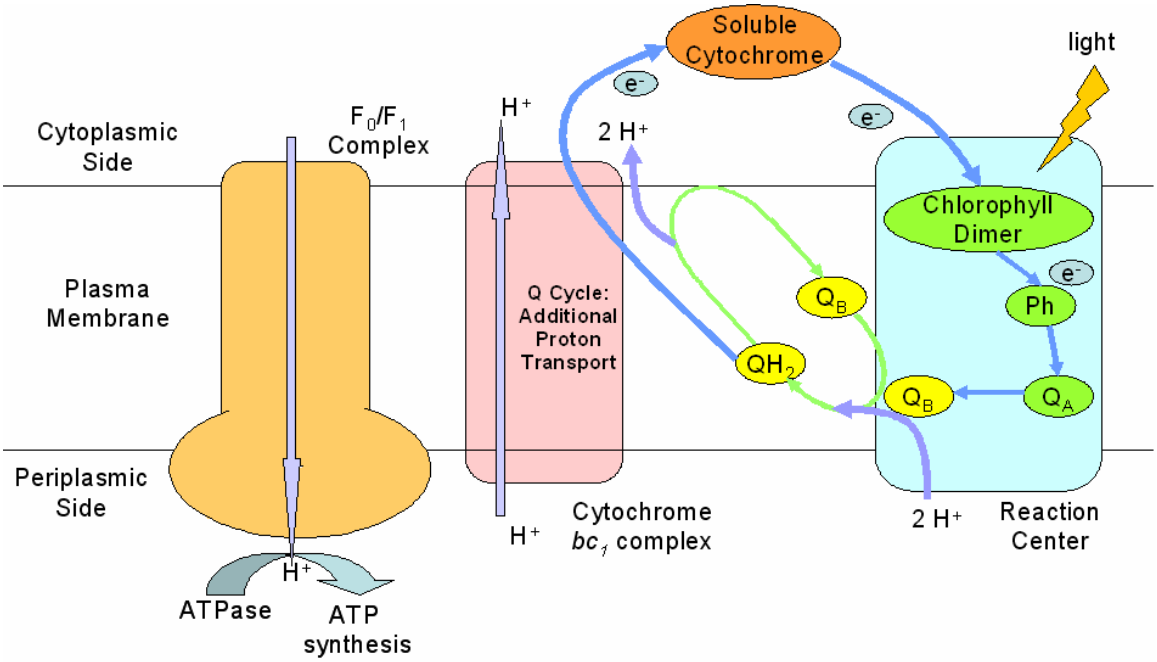

Figure 1.3 The pathway of cyclic photosynthesis in the purple bacteria. The special pair P870 is excited by light and oxidized. At each turnover, only one electron can be transferred. One cytochrome c is oxidized on each turnover. The electron transfers from P to H_L, to Q_A then Q_B. After 2 turnovers, with acceptance of two electrons and two protons, the dihydroquinone Q_BH_2 dissociates from RCs. Cytochrome bc1 complex then transfers electrons from Q_BH_2 to soluble cytochrome c on the cytoplasmic side of the membrane. The soluble cytochrome c re-reduces the special dimer P870 and starts a new reaction cycle.

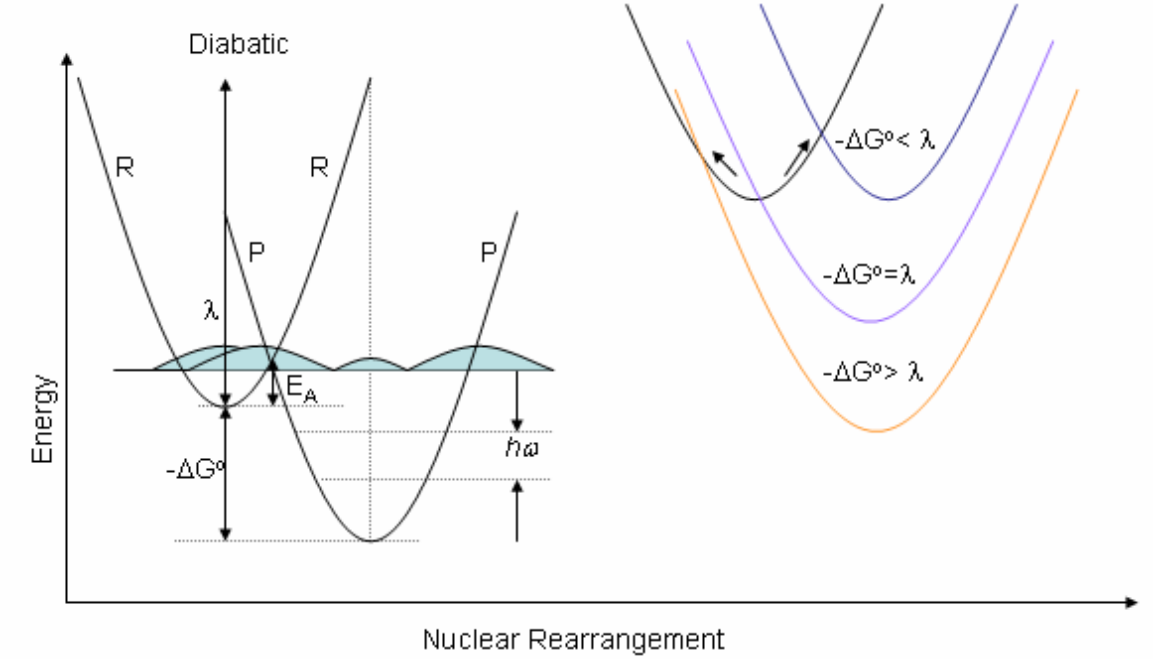

Figure 1.4. The equilibrium geometry corresponds to the bottom of the potential well. Electrons tunnel from the reactant state R down to the acceptor, the reactant state is DA and product state D^+A^-. Nuclear vibrations are treated as a harmonic oscillator. In the quantized view, the harmonic oscillator potential is spaced by the quantum energy of the oscillator hω. Nuclear tunneling from reactant to product depends on the overlap of the harmonic oscillator wave functions. The activation energy E_A depends on the free energy of the reaction and the reorganization energy of reaction. When $-\Delta G^o = \lambda$, the activation energy EA is zero, the electron transfer rate k_{et}^o is maximum; when $-\Delta G^o < \lambda$ (The normal region) and $-\Delta G^o > \lambda$ (the Marcus inverted region), the activation energy is non-zero and k_{et} is slower.

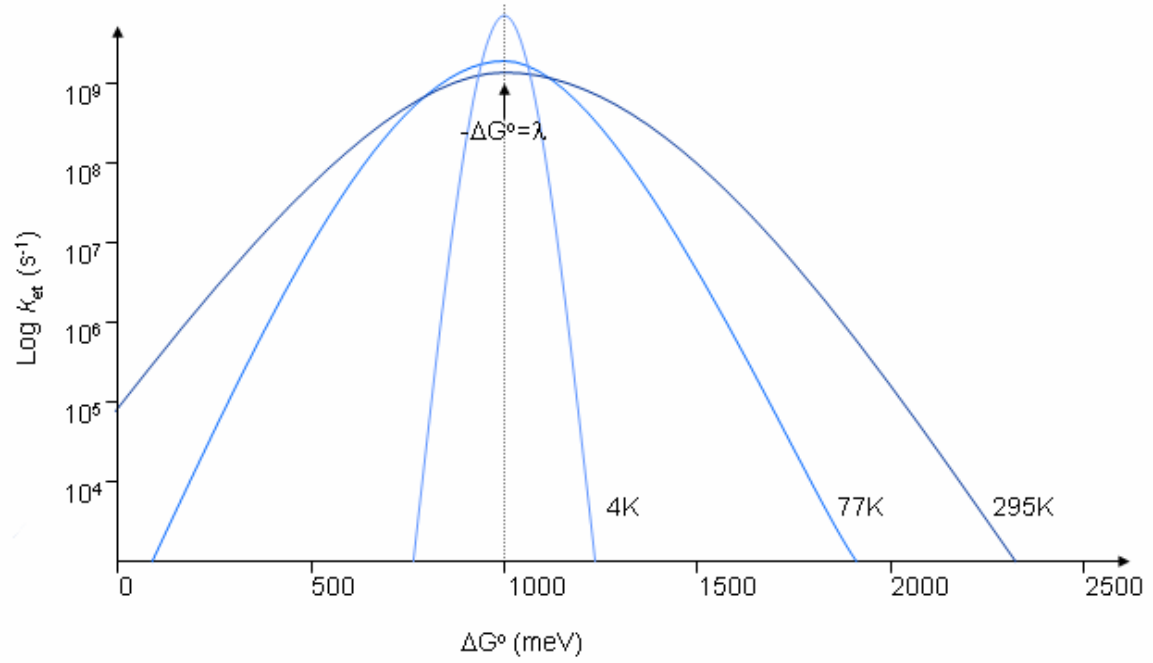

Figure 1.5 Temperature sensitivity of the electron transfer rate depends on the free energy. λ is assumed to be 1000 meV here. Only at $-\Delta G^o = \lambda$, is the activation energy ($E_A = \frac{(-\Delta G^o - \lambda)^2}{4\lambda}$) zero, the electron transfer rate k_{et}^o is fastest and it increases as the temperature is lowered.

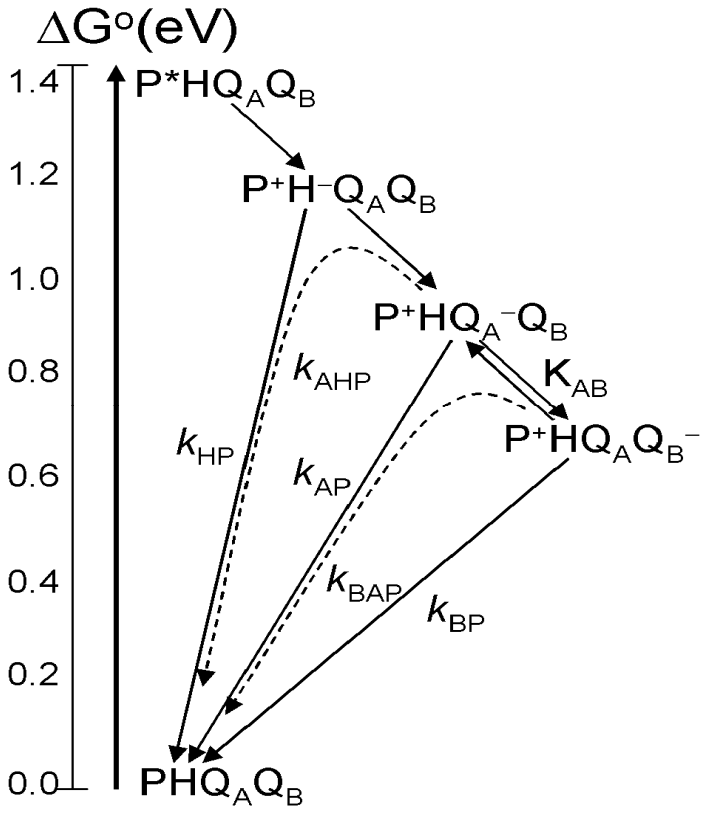

Figure 1.6 Electron transfer pathway in the *Rb. Sphaeroides* reaction centers. The darker arrow shows the forward pathway, whereas the dashed arrows show routes for the uphill thermal back reaction charge recombination processes. First an electron on P is promoted to the excited singlet state (P*) by absorption of a photon. Initial charge separation, over 15 Å to H with $-\Delta G^o \approx 160$ meV, occurs in 3 ps forming P^+H^-. In 200 ps, the electron moves to the primary quinone Q_A, 10.1 Å from H with $-\Delta G^o \approx 670$ meV. The secondary quinone Q_B accepts the electron from Q_A^-, 14.5 Å from Q_A with $-\Delta G^o_{AB} \approx 60$ meV. This step occurs in 3-200 μs to form $P^+Q_B^-$. If there is no external donor to donate an electron to P^+, the electron on the acceptors will go back to P^+ in a charge recombination back reaction. There are two types of charge recombination pathways: thermal back reaction and direct tunneling reaction. The direct back reaction rate from Q_A^- or Q_B^- to P^+ (22.5 and 23.4 Å respectively) is represented as k_{AP} or k_{BP}; k_{AHP} or k_{BAP} are the indirect thermal

back reaction rates to P^+ via a higher energy state. The intermediate state is $P^+H^-Q_A$ for $P^+Q_A^-$ and $P^+Q_A^-Q_B$ for $P^+Q_B^-$.

References

Allen, J. P., G. Feher, et al. (1987). "Structure of the reaction center from *Rhodobacter sphaeroides* R-26: The cofactors." Proc. Natl. Acad. Sci. USA 84: 5730-5734.

Allen, J. P., G. Feher, et al. (1987). "Structure of the reaction center from *Rhodobacter sphaeroides* R-26: The protein subunits." Proc. Natl. Acad. Sci. USA 84: 6162-6166.

Allen, J. P., G. Feher, et al. (1988). "Structure of the reaction center from *Rhodobacter Sphaeroides* R-26 and 2.4.1." 5-11.

Allen, J. P., G. Feher, et al. (1988). "Structure of the reaction center from *Rhodobacter sphaeroides* R-26: Protein-cofactor (quinones and Fe^{+2}) interactions." Proc. Natl. Acad. Sci. USA 85: 8487-8491.

Allen, J. P., J. C. Williams, et al. (1998). "Free energy dependence of the direct charge recombination from the primary and secondary quinones in reaction centers from *Rhodobacter sphaeroides*." Photosynth. Res. 55: 227-233.

Baccarini-Melandri, A., N. Gabellini, et al. (1980). "Structural requirements of quinone coenzymes for endogenous and dye-mediated coupled electron transport in bacterial photosynthesis." J Bioenerg Biomembr 12(3-4): 95-110.

Blankenship, R. E. (1992). "Origin and early evolution of photosynthesis." Photosynth Res 33: 91-111.

Blankenship, R. E., M. T. Madigan, et al. (1995). Anoxygenic Photosynthetic Bacteria, Kluwer Academic Publishers.

Chang, C.-H., O. El-Kabbani, et al. (1991). "Structure of the membrane-bound photosynthetic reaction center from *Rhodobacter sphaeroides*." Biochemistry 30: 5352-5360.

Chang, C. H., D. Tiede, et al. (1986). "Structure of *Rhodopseudomonas sphaeroides* R-26 reaction center." FEBS Lett. 205: 82-86.

Clayton, R. K. (1980). Photosynthesis: physical mechanisms and chemical patterns. Cambridge, Cambridge University Press.

Clayton, R. K. and R. T. Wang (1971). "rc prep." Methods Enzymol 23: 696-704.

Cramer, W. A. and D. B. Knaff (1991). Energy Transduction in Biological Membranes: A Textbook of Bioenergetics. New York, Springer-Verlag.

Deisenhofer, J., O. Epp, et al. (1984). "X-ray structure analysis of a membrane protein complex: Electron density map at 3 Angstroms resolution and a model of the chromophores of the photosynthetic reaction center from *Rhodopseudomonas viridis*." J. Mol. Biol. 385: 385.

Deisenhofer, J., O. Epp, et al. (1985). "Structure of the protein subunits in the photosynthetic reaction center of *Rhodopseudomonas viridis* at 3 Å resolution." Nature 318: 618-624.

Deisenhofer, J. and H. Michel (1989). "The photosynthetic reaction center from the purple bacterium *Rhodopseudomonas viridis*." Science 245: 1463-1473.

Deisenhofer, J. and H. Michel (1989). "The photosynthetic reaction centre from the purple bacterium *Rhodopseudomonas viridis*." The EMBO Journal 8: 2149-2170.

Feher, G., J. P. Allen, et al. (1989). "Primary processes in bacterial photosynthesis: Structure and function of bacterial photosynthetic reaction centres." Nature 339:111-116.

Giangiacomo, K. M. and P. L. Dutton (1989). "In photosynthetic reaction centers, the free energy difference for electron transfer between quinones bound at the primary and secondary quinone-binding sites governs the observed secondary site specificity." Proc. Natl. Acad. Sci. USA 86: 2658-2662.

Graige, M. S., G. Feher, et al. (1998). "Conformational gating of the electron transfer reaction $Q_A^- Q_B$ $Q_A Q_B^-$ in bacterial reaction centers of *Rhodobacter sphaeroides* determined by a driving force assay." Proc. Natl. Acad. Sci. USA 95: 11679-11684.

Gunner, M. R. (1991). "The reaction center protein from purple bacteria: Structure and function." Current Topics in Bioenergetics 16: 319-367.

Gunner, M. R., B. S. Braun, et al. (1985). The characterization of the Q_A binding site of the reaction center of *Rhodopsuedomonas sphaeroides*. Antenna and Reaction Centers of Photosynthetic Bacteria. M. E. Michel-Beyerle. New York, Springer-Verlag: 298-305.

Gunner, M. R. and P. L. Dutton (1989). "Temperature and $-\Delta G^o$ dependence of the electron transfer from BPh- to Q_A in reaction center protein from *Rhodobacter sphaeroides* with different quinones as Q_A." J. Am. Chem. Soc. 111: 3400-3412.

Gunner, M. R., D. E. Robertson, et al. (1986). "Kinetic studies on the reaction center protein from *Rhodopseudomonas sphaeroides: T*he temperature and free energy dependence of electron transfer between various quinones in the Q_A site and the oxidized bacteriochlorophyll dimer." J. Phys. Chem. 90: 3783-3795.

Gunner, M. R., D. M. Tiede, et al. (1982). Quinones as prosthetic groups in membrane electron-transfer proteins I: Systematic replacement of the primary ubiquinone of photochemical reaction centers with other quinones. Function of Quinones in Energy Conserving Systems. B. L. Trumpower. New York, Academic Press: 265-269.

Heathcote, P. (2002). "Reaction centers: the structure and evolution of biological solar power." Trends Biochem Sci 27: 79-86.

Kirmaier, C. and D. Holten (1987). "Primary photochemistry of reaction centers from photosynthetic purple bacteria." Photosynthesis Research 13: 225-260.

Kirmaier, C. and D. Holten (1993). Electron transfers and charge recombination reactions in wild type and mutant bacterial reaction centers. The Photosynthetic Reaction Center. J. Deisenhofer and J. R. Norris. San Diego, Academic Press. II: 49-70.

Kleinfeld, D., M. Y. Okamura, et al. (1984). "Electron transfer in reaction centers of *Rhodopseudomonas sphaeroides:* I. Determination of the charge recombination pathway of $D^+Q_AQ_B^-$ and free energy and kinetic relations between Q_A-Q_B and Q_AQ_B-." Biochim. Biophys. Acta 766: 126-140.

Kleinfeld, D., M. Y. Okamura, et al. (1984). "Electron-transfer kinetics in photosynthetic reaction centers cooled to cryogenic temperatures in the charge separated state: Evidence for light-induced structural changes." Biochemistry 23: 5780-5786.

Kuglstatter, A., J. Miksovska, et al. (2000). "Structure of the photosynthetic reaction centre from *Rhodobacter sphaeroides* reconstituted with anthraquinone as primary quinone Q(A)." FEBS Letts. 472: 114-6.

Lancaster, C. R. D. (1998). "Ubiquinone reduction and protonation in photosynthetic reaction centres from *Rhodopseudomonas viridis:* X-ray structures and their functional implications." Biochim. Biophys. Acta 1365: 143-150.

Li, J., E. Takahashi, et al. (2000). "$-\Delta G^o_{AB}$ and pH dependence on the electron transfer from $P^+Q_A^-Q_B$ to $P^+Q_AQ_B^-$ in *Rhodobacter sphaeroides* reaction centers." Biochemistry 39: 7445-7454.

Mancino, L. J., D. P. Dean, et al. (1984). "Kinetics and thermodynamics of the $P870^+Q_A^-$ to $P870^+Q_B^-$ reaction in isolated reaction centers from the photosynthetic bacterium *Rhodopseudomonas sphaeroides."* Biochim. Biophys. Acta 764: 46-54.

Marcus, R. A. and N. Sutin (1985). "Electron transfers in chemistry and biology." Biochim. Biophys. Acta 811: 265-322.

McMahon, B. H., J. D. Muller, et al. (1998). "Electron transfer and protein dynamics in the photosynthetic reaction center." Biophys. J. 74: 2567-2587.

Millsaps, J. F., B. D. Bruce, et al. (2001). "Nanoscale photosynthesis: photocatalytic production of hydrogen by platinized photosystem I reaction centers." Photochem Photobiol 73(6): 630-5.

Moser, C. C., J. M. Keske, et al. (1992). "Nature of biological electron transfer." Nature 355: 796-802.

Okamoto, Y. (1994). "Dependence on the Dielectric Model and pH in a Synthetic Helical Peptide Studied by Monte Carlo simulated Annealing." 529-539.

Okamura, M. Y., G. Feher, et al. (1982). Reaction centers. Photosynthesis: Energy conversion by Plants and Bacteria. Govindjee. New York, Academic Press. 1: 195-272.

Okamura, M. Y., R. A. Isaacson, et al. (1975). "The primary acceptor in bacterial photosynthesis: Obligatory role of ubiquinone in photoactive reaction centers of *Rhodopseudomonas sphaeroides.*" Proc. Natl. Acad. Sci. USA 72: 3492-3496.

Peter Raven., R. E., Susan Eichhorn (1999). Biology of Plants, W.H. Freeman and Company.

Pokkuluri, P. R., P. D. Laible, et al. (2004). "Temperature and cryoprotectant influence secondary quinone binding position in bacterial reaction centers." FEBS Lett 570(1-3): 171-4.

Shopes, R. J. and C. A. Wraight (1985). "The acceptor quinone complex of *Rhodopseudomonas viridis* reaction centers." Biochim. Biophys. Acta 806: 348-356.

Stowell, M. H. B., T. M. McPhillips, et al. (1997). " Light-induced structural changes in photosynthetic reaction center: implications for mechanism of electron-proton transfer." Science 276: 812-816.

Wang, Z., C. J. Medforth, et al. (2004). "Porphyrin nanotubes by ionic self-assembly." J Am Chem Soc 126(49): 15954-5.

Williams, J. C., L. A. Steiner, et al. (1986). "Primary structure of the reaction center from *Rhodopseudomonas sphaeroides*." Proteins: Struct. Funct. Genet. 1: 312-325.

Woodbury, N. W. and J. P. Allen (1995). The pathway, kinetics and thermodynamics of electron transfer in wild type and mutant reaction centers of purple nonsulfur bacteria. Anoxygenic Photosynthetic Bacteria. R. E. Blankenship, M. T. Madigan and C. E. Bauer. Dordrecht, Kluwer.

Woodbury, N. W., W. W. Parson, et al. (1986). "Radical-pair energetics and decay mechanisms in reaction center containing anthraquinones or benzoquinones in place of ubiquinone." Biochim. Biophys. Acta. 851: 6-22.

Wraight, C. A. and R. R. Stein (1983). Bacterial reaction centers as a model for photosystem II: Turn over of the secondary acceptor quinone. The oxygen evolving system of photosynthesis. Y. Inoue, A. R. Crofts, Govindjeeet al. New York, Academic: 383-393.

Zubay, G. (1988). Biochemistry. New York, Macmillan.

Materials and Methods

2.1 Protein Preparation

The purple non-sulfur photosynthetic bacteria *Rhodobactor sphaeroides* were used for the experiments reported here. Reaction centers are an engineered poly-histidine tagged and carotenoid containing protein, provided by Dr. Philip D. Laible (Argon National lab). External conditions are important to culture *Rb. Sphaeroides* bacteria so they have a good yield of poly-histidine tagged proteins. The *Rb. Sphaeroides* bacteria are grown anaerobically without light at 34^{o}C. A shaker speed of 125 RPM provides the right amount of oxygen in the media. Bacteria grown in the dark rely on aerobic respiration for energy. However, if there is too much oxygen, the photosynthetic apparatus is not made. The culture starts in 125ml bottle, than is transferred to a 2.8L Fernbach flask with 2 liters YCC media. It takes 2-3 days for bacteria to grow to a sufficient density to harvest.

The photosynthetic apparatus including the photochemical reaction centers is carried in and on the protein-phospholipid cell membranes. A french pressure cell press is used to disrupt the cells. The cell plasma membrane and cell walls of bacteria are broken by passing them through a narrow valve under 20,000psi high pressure. The cytoplasmic and intracytoplasmic membranes are fragmented, and fragments reform into sealed round vehicles. The fragmented phospholipid membranes exist in solution as chromatophores formed by the invagination of the inner cytoplasmic membrane. The chromatophores can be isolated by centrifugation in the supernatant. The resuspended chromatophores are exposed to the detergent Lauryl dimethyl amine oxide (LDAO), which replaces the lipid

molecules surrounding reaction centers and antenna complexes in chromatophores, solubilizing them.

After the protein/detergent complexes are solubilized, they are separated from the pellet membrane debris by high-speed centrifugation, which gets rid of any unsolubilized membrane and larger particles. It was found that skipping this step does not affect RC yield or purity. Column chromatography with Nitrilo-Tri-Acetic acid (Ni-NTA) is used to separate the reaction centers from the remaining proteins. His-tagged reaction centers bind to the Ni cation on the column by chelation. RCs were purified on Ni-NTA (nitrilotriacetic acid) resin. The Ni-NTA column was prepared with 0.05% LDAO in 10mM Tris buffer (pH 7.8) and the reaction centers were eluted with 40 mM imidazole in 0.05% LDAO at pH 7.8. The imidazole has a structure similar to histidine; hence it competitively binds the Ni to displace the protein from the column. Reaction centers and imidazole are collected. The imidazole is removed from the reaction centers by dialysis before storing. The yield of protein purification at this step is around 90%. Native ubiquinone at both sites are reserved. To increase the purity of the reaction centers, a diethylaminoethyl cellulose (DEAE) column is used after dialysis. The DEAE column is an anion exchange column and NaCl is used to elute the protein. The final step is dialysis of the supernatant that comes from the DEAE column at 4^{o}C for 24 hours (McPhalen and James 1987; Goldsmith and Boxer 1996). The overall yield of the reaction centers found after the DEAE column related to that after French Press step is ~ 50%.

In order to probe the factors that control electron transfer, different quinones can be substituted for the native quinone at the Q_A binding site. Q_A was removed by washing the reaction centers by chromatography on the DEAE-cellulose column. The DEAE column is pretreated with bovine serum albumin (BSA) to mask hydrophobic binding sites, saturating this non-specific binding sites while keeping the ion binding sites exposed. The reaction centers were mixed in the column with ≈ 1mg BSA per ml of DEAE material. The column was washed with 4% LDAO, 10 mM 1,10-phenanthroline, and 10 mM Tris at 28°C for 2 hours. The yielded protein with 90-95% of the native ubiquinone-10 at Q_A and all of the Q_B removed (Okamura, Isaacson et al. 1975; Woodbury, Parson et al. 1986). RCs with a single quinone in the Q_A site were prepared using the same column processes at 25°C. In the Q_B-deleted RCs, Q_A is saturated with 100% ubiquinone-10. There is no ubiquinone at the Q_B site. The yield of quinone-deleted reaction centers is around 50%. The protein was stored in 10mM Tris, pH 7.8, 0.05% LDAO at -80°C. The RC concentration was determined given $\varepsilon_{802} = 0.288\ \mu M^{-1} \cdot cm^{-1}$.

2.2 Quinone Reconstitution

Quinones are dioxo derivatives of dihydroaromatic systems: Benzoquinone, Naphthoquinone and Anthraquinone are typical examples.

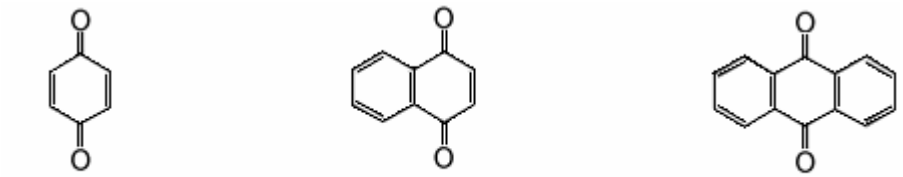

Most quinones used here were purchased commercially. Ubiquinone-1 (UQ-1, 2,3-dimethoxy, 5-methyl benzoquinone), Ubiquinone-10 (UQ-10), 1, 4-Naphthoquinone (NQ), 9, 10-Anthraquinone (AQ) and 2, 6-Dimethyl-Benzoquione (DmBQ), Duroquinone (DQ), 2-Methyl-1,4-Naphthoquinone (2mNQ) 2,3-Dimethyl-1,4-Naphthoquinone (DmNQ) and 2-methyl, 1,4-Naphthoquinone are purchased from Sigma. Trimethylquinone (TMBQ) was purchased from Pfaltz & Bauer, Inc. All quinones were dissolved in ethanol. The anthraquinone concentration is defined by spectrum with ε_{250} = $45mM^{-1}cm^{-1}$.

Ubiquinones with tails shorter than four isoprene units are dissolved in ethanol. The long-tailed ubiquinones are effectively insoluble in water, but become soluble when detergent is added. However, detergent weakens the affinity of quinone for the binding sites (McComb, Stein et al. 1990). Dissolving the quinone in 2% Triton X-100 permits effective and reproducible reconstitution of long-tailed quinones (McComb, Stein et al. 1990). The relatively insoluble UQ-10 stock solution was heated for 5 seconds in a microwave oven before being added to reaction centers. Stock solutions were stable for months when stored in the dark at -20^{o}C.

For measurement at room temperature (298 ± 2K), the protein concentration is usually controlled around 1μM. The sample contains 10mM Tris, pH 8.0, 0.005% LDAO which is below the critical micelle concentration of 0.05% (2.1mM) (McComb, Stein et al. 1990). Non-native quinones are added up to their solubility limit of ~1 mM.

2.3 Instrumentation

Light-induced changes of absorbance allow the electron transfer reaction in reaction centers to be measured. The cofactors in reaction centers absorb light differently in the difference redox state. A flash of light that forms P+QA- induces an absorbance changes with maximum 430 nm (Figure 2.2 & 2.3). The light saturation of flash is around 90% (Figure 2.8). The amplitude of the absorption changes show how much P^+ is formed. The rate of return to the ground state show if the electron has reached H, Q_A or Q_B (Figure 2.5) In absorbance measurement, the relationship between the transmittance (T) and the optical density (O.D.) is

$$O.D. = \log_{10}(1/T)$$

The ideal absorbance of a dilute solute in a transparent solvent conform to the Lambert-Bouguer-Beer Law:

$$A=\varepsilon cd=\log_{10}(I_0/I_x)$$

ε is the molar extinction coefficient of the solute, its unit is $ml \cdot mM^{-1} \cdot cm^{-1}$. c is the concentration of the solute, the unit is $mM \cdot ml^{-1}$. d is the optical path length in cm. I_0 is the initial light intensity before passing through the sample. I_x is the light intensity after passing through the sample, ε is the optical density specific to the solute.

The specific concentration of the reaction centers is obtained by measuring the absorbance. The absorption spectra of isolated RCs in *Rhodobacter Sphaeroides* are taken by a JASCO V-530 UV spectrometer from 250 nm to 1000 nm (Figure 2.2). The concentration of the reaction centers is determined optically using the extinction coefficient: $\varepsilon_{802}=0.288\ \mu M^{-1} \cdot cm^{-1}$(Straley, Parson et al. 1973).

The absorbance transient is measured by a flash spectrophotometer designed by the University of Pennsylvania Biomedical Instrumentation Group (Figure 2.1). The excitation light is provided by 10 μs flash from a xenon flash lamp. The measuring light that controlled by the monochromator is perpendicular to the excitation flash light. The measuring light is provided by a 100W quartz-halogen-tungsten lamp (ORIEL) with neutral density and interference filters. Measurements are made at 430 nm is because the P^+ absorption changes signal has a maximum here (Figure 2.3). The transmitted light is detected by a Thorn EMI 9798QB photomultiplier. The signal is monitored using a LeCroy 9310M (300 MHz) or 9310A (400 MHz) oscilloscope after it is amplified and filtered. The digital storage oscilloscopes are used to record and average the kinetic transients at different time scales.

2.4 Data Analysis

The occupancy of the binding sites is determined from the kinetics of charge recombination. The observed $P^+Q_A^-$ or $P^+Q_B^-$ of decay to the ground state, rate is different for each quinone at each binding site. The charge recombination kinetics are analyzed by a nonlinear least-squares fitting program in Igor Pro from WaveMetrics. The kinetic traces are fit to 2 or 3 exponentials plus a constant using the standard expression:

$$A(t) = A_0 + A_1 \times \exp(-t/\tau_1) + A_2 \times \exp(-t/\tau_2) + A_3 \times \exp(-t/\tau_3) \quad (2.1)$$

Where A refers to amplitude, τ represents decay time.

Charge recombination from $P^+Q_A^-$ to PQ_A occurs as a nearly single exponential with a rate constant (k_{AP}^{obs}) which is characteristic of the quinone (Gunner and Dutton 1989). These kinetic traces are analyzed by a single exponential plus one constant. When

both quinone sites are occupied with a functional quinone, but not 100% saturated at the Q_B site, electrons returns to the ground state from both Q_A and Q_B sites. The charge recombination rates k_{AP}^{obs} and k_{BP}^{obs} are distinguishable. The k_{BP}^{obs} is slower than k_{AP}^{obs}. The fitting curve now includes two exponentials plus a constant. With a saturated Q_B site, the yield for $P^+Q_B^-$ is close to 100%. The electrons transfer from Q_B to Q_A then back to ground state at a single rate, so the kinetic trace can be analyzed by a single exponential plus a constant (Figure 2.5). In the reaction centers with different quinones, the fitting can be modified with additional exponential phases as needed. The residual error for calculating with different members of exponential are compared to select the best fitting procedure for kinetic traces, looks for systematic difference between the selected fitting curve and the original kinetic data (Figure 2.5).

The time range of the experiment depends on the observed back reaction rate. Two digitizing oscilloscopes are used to record two sets of data simultaneously, one is for shorter times, and the other is for longer times. The rate of the fastest reaction is obtained from the shorter time measurement. The rate constant is fix when the longer trace is analyzed.

2.5 Measurement of Quantum Yield Φ_Q for Low Potential Q_A

The Quantum Yield is a measure of the efficiency with which absorbed light produces some effect. In the photosynthetic reaction centers, the quantum yield refers to the fraction of reaction centers in which the electron is transferred to the next acceptor compared other than returning to the ground state.

$$\Phi = \frac{RC_{electronforward}}{RC_{electronforward} + RC_{electronreturn}} \qquad (2.2)$$

The quantum yield is less than 1 if not all electrons move forward to next electron acceptor.

The quantum yield Φ for $P^+Q_A^-$ measures how much of the P^+H^- formed by the actinic flash goes either forward to the $P^+Q_A^-$ state (k_{HA}) or returns to the ground state (k_{HP}). The absolute quantum yield of native reaction centers with ubiquinone at Q_A (Φ_{HQ}) has previously been measured to be 1.02±0.04 (Loach and Sekura 1968; Wraight and Clayton 1973). Give the ratio of the rates k_{HA} and k_{HP}. Φ_{HA} for UQ_A should be 0.984 at room temperature. The quantum yield Φ of other quinones by comparing their yield relative to that found with native reaction centers. The quantum yield is measured by the multiflash method. The time interval between two continuous flashes is 100ms if the back reaction rate k_{AP} is slow enough that a second flash can be administered before the protein has return to the ground state.

Two methods are used to measure Φ_{HQ}. Here Φ_{HQ} of the protein form $P^+Q_A^-$ after the first flash while $(1-\Phi_{HA})$ is the fraction that returns to the ground state. If there were no return to the ground state between flashes and additional $\Phi_{HA}\cdot(1-\Phi_{HA})$ of the protein forms $P^+Q_A^-$ after the next flash. After each flash (Φ_{HA}) of the reaction centers in the ground state is accumulated to the $P^+Q_A^-$ population.

The quantum yield can be delivered in these reaction centers where low potential quinone in the Q_A site form a $P^+Q_A^-$ state where electrons return to the ground state before another flash. It was determined by light saturation method (Gunner and Dutton 1989). Kodak neutral density filters (0.1 – 2.5 N.D.) were used to attenuate the light intensity of the excitation at 430nm.

$$[P^+Q_A^-] = [P^+Q_A^-]_{\max} \cdot (1 - \exp[-\Phi_Q(kI')t]) \qquad (2.3)$$

The amount of $P^+Q_A^-$ is obtained from the absorbance change of P^+, I' is the relative intensity of the flash with each filter, which should be proportional to the number of photons absorbed by reaction centers, $I' = (2 \times Tr_{804} + Tr_{865})/3$. The transmittance (Tr) are measured at the two wavelengths for the proteins absorbance maximum in the near-IR. The transmittance data are obtained by JASCO 530 UV/VIS spectrometer. I' without neutral density filter is defined as 1.0.

The quantum yield of $P^+Q_B^-$, Φ, is the fraction of reaction centers that $P^+Q_B^-$ from $P^+Q_A^-$. The quantum yield is determined from the amplitude of the slow (A_S) and fast (A_F) components of the P^+ charge recombination (Figure 2.4).

$$\Phi_{AB} = \frac{A_s}{A_s + A_F} = \frac{[P^+Q_B^-]}{[P^+Q_B^- + P^+Q_A^-]} \qquad (2.4)$$

The rate of electron transfer from Q_A^- to Q_B (k_{AB}) can be obtained from the quantum yield Φ for forming $P^+Q_B^-$.

$$\Phi_{AB} = \frac{A_s}{A_s + A_F} = \frac{k_{AB}}{k_{AB} + k_{AP}} \qquad (2.5)$$

k_{AB} is given the observed back reaction rate, k_{AP}^{obs}, in the absence of Q_B (Li, Takahashi et al. 2000). Given the reactant $P^+Q_A^-$ decays at $k_{AP} + k_{AB}$, k_{AB} can not be measured when $k_{AB} << k_{AP}$ since no $P^+Q_B^-$ is formed. When $k_{AB} \approx k_{AP}$ (Vermeglio and Clayton 1977; Wraight 1979; Kleinfeld, Okamura et al. 1984; Graige, Feher et al. 1998), k_{AB} can be obtaining most accurately from the quantum yield Φ. k_{AB} may be measured directly from the rate of formation of $P^+Q_B^-$ when $k_{AB} >> k_{AP}$.

2.6 Methods to Determine Q_A and Q_B Reconstitution

Reduction kinetics of flash-induced P^+. The occupancy of each binding site is determined by the kinetics of the charge recombination. If there is no Q_A, P^+H^- returns to the ground state in 10ns so no signal is seen. Therefore occupancy in the site is proportion to the absorption change for P^+. If Q_A is saturated with quinone, the total absorption change of P^+ is independent of whether Q_B is functional or not. However, the charge recombination rate from quinone at the Q_B site, k_{BP}^{obs}, always slower than k_{AP}^{obs}. Thus, the observation of a slow phase k_{BP}^{obs} shows the reconstitution of functional quinone at the Q_B site. The fraction of slow phase increases with more functional Q_B reconstitution. For reaction centers with UQ at both sites, k_{AP} ($10s^{-1}$) is 100 times faster than k_{BP} ($0.1s^{-1}$) (Xu and Gunner 2001).

The $P^+Q_A^-$ or $P^+Q_B^-$ decay rates are different for each quinone. However, with different quinones at Q_A or Q_B sites, the back reaction rate is the same at different wavelengths (Figure 2.6). For examples, the absorbance changes of P^+ at 430 nm are larger than those at 550nm as expected given the P+-P difference absorbance spectra (Figure 2.3).

Cytochrome c oxidization of reaction centers on the second and first flashes. Cytochrome c extracted from horse heart (Sigma) is reduced by sodium dithionite in PD-10 column. The reduced cytochrome c has a sharp absorption peak near 550 nm that not exist in the oxidized form. The extinction coefficient at 550 nm for reduced cytochrome c is 27.6 mM^{-1} cm^{-1}. Therefore cytochrome c oxidization is measured at 550 nm where cyt^{2+} (reduced) –cyt^{3+} (oxidized) shows a maximum absorption change.

Cytochrome c acts as an external electron donor to reduce the oxidized P^+. This is not dependent of the Q_B. The electron transfer rate from cytochrome c to P^+ (1~2 μs) is much faster than the charge recombination rate from $P^+Q_A^-$ (100 ms). With the reduced semiquinone Q_A^-, no secondary electron acceptor Q_B, the cytochrome c oxidization only occurs on the first flash (Parson 1969):

$$Cyt_{red} + P^+Q_A^- \rightarrow Cyt_{oxi} + PQ_A^-$$

With successive flashes, extra electrons can not be added to the reduced Q_A. The reaction centers with PQ_A^- are inactive on the time scale of the reaction with oxidized cytochrome c. After a flash P^+H^- undergoes change recombination before the cytochrome can reduce P^+. In the present of functional Q_A and Q_B, additional cytochrome c oxidization can occur only after the electron has transferred from Q_A^- to Q_B with the second flash. The ratio of second/first flash cytochrome c oxidization is dependent on the occupancy of a functional Q_B. The free energy between Q_A and Q_B is important since ratio $P^+Q_AQ_B^-$ and $P^+Q_A^-Q_B$ depends on the equilibrium constant for electron transfer for $Q_A^-Q_B$ to $Q_AQ_B^-$ (Kleinfeld,

Okamura et al. 1984); (Halsey and Parson 1974) . For reaction centers with one UQ_A and one UQ_B, the mixture of UQ_AUQ_B states present after the first two flashes are shown:

First flash: $Cyt_{red} + PQ_AQ_B \rightarrow Cyt_{oxi} + (PQ_A^-Q_B \xleftrightarrow{K_{eq}} PQ_AQ_B^-)$

Second flash: $Cyt_{red} + PQ_AQ_B^- \rightarrow Cyt_{oxi} + (PQ_AQ_B^- \xleftrightarrow{K_{eq}} PQ_AQ_B^{2-})$

$$Cyt_{red} + PQ_A^-Q_B \rightarrow \text{No Reaction}$$

The ratio of second/first flash of cytochrome c with UQ_AUQ_B bound reaction centers is equal to 1 if K_{eq} is sufficiently comparable (Figure 2.8). The electron at $PQ_A^-Q_B^-$ can transfer to $PQ_AQ_B^{2-}$ in 100~200μs. The $P^+Q_A^-Q_B^{2-}$ can oxidize the third cytochrome c. The amount of oxidized cytochrome c is the same after each flash. The quinone at Q_A can accept only one electron, at Q_B can accept 2 electrons. Therefore, if there is no external quinone added to replace the fully reduced Q_B, with 4th flash, the charge separation can not happens, so there is no more oxidized cytochrome c generated. Therefore, even with more flashes, the absorbance changes of oxidized cytochrome c keeps stay.

2.7 Determining the Affinity of Active Quinones at the Q_A or Q_B Sites.

With the addition of external quinones to the empty quinone site in reaction centers, the dissociation constant K_d can be determined. Not all quinones are functional. When a quinone is added to a solution of reaction centers with empty Q_A or Q_B site, there are three possibilities:

- The quinone doesn't bind.
- The quinone binds but is not functional as an electron acceptor.
- The quinone binds and reconstitutes function.

For a quinone can functional binding to reaction centers, the equation that describe equibrium binding are:

$$RC_{Free} + Q_{Free} \rightarrow RC \cdot Q$$

$$RC_{Total} = RC_{Free} + RC \cdot Q$$

$$Q_{Total} = Q_{Free} + RC \cdot Q$$

Where RC_{Total} and Q_{Total} are total concentration of added reaction centers and quinone; RC_{Free} and Q_{Free} are the unassociated reaction centers and quinone; $RC \cdot Q$ is reaction centers bound with quinone. This method determines the quinone binding to reaction centers prior to the flash. The dissociation constant is given by the standard binding equation:

$$K_d = \frac{[RC_{Free}][Q_{Free}]}{[RC \cdot Q\ ]} \quad (2.6)$$

If the quinone is a functional electron acceptor at the Q_A site the [RC·Q] derived from the absorbance change of P^+. As more functional quinone is bound to reaction center ($RC \cdot Q$), the absorbance changes due to P^+ increases. The amplitude of the ΔA_{430} is directly proportional to the ($RC \cdot Q$) concentration:

$$[RC \cdot Q] = \left(\frac{\Delta A - \Delta A_{\min}}{\Delta A_{\max} - \Delta A_{\min}} \right) \cdot RC_{Total} \quad (2.7)$$

Where ΔA_{min} is the flash induced amplitude change found before quinone addition due to the 5-10% residual Ubiquinone-10 left in the Q_A site. ΔA_{max} is the amplitude when all RCs have bound a functional quinone. The best fit for the dissociation constant (K_d) was determined from equation (2.8) using the dependence of ΔA_{430} on the total quinone

concentration (Q_T) using the Levenberg-Marquardt fitting program in IGOR Pro (WaveMetrics). The binding curve for a functional quinone titration is drawn with Q_{Total} as X-axis and $\Delta A(Q_T)$ as the Y-axis (Figure 2.4).

$$\Delta A(Q_T) = \frac{1}{2}\left\{\left(1+\frac{[Q_{Total}]+K_d}{[RC_{Total}]}\right)-\sqrt{\left(1+\frac{[Q_{Total}]+K_d}{[RC_{Total}]}\right)^2-4\frac{[Q_{Total}]}{[RC_{Total}]}}\right\}\cdot(\Delta A_{\max}-\Delta A_{\min}) \tag{2.8}$$

The binding curve shifts to right with looser binding affinity and a larger K_d of the functional quinone.

2.8 Competitive Inhibition as a Measure of the Affinity of Quinones for the Q_A or Q_B Sites.

For non-functional quinones bound to reaction centers, a competitive inhibition assay is used to measure the quinone binding affinity. In this method, the non-functional quinone is a competitive inhibitor of binding of a functional quinone. In competitive inhibition, both quinones bind to the same site, so both cannot bind at the same time. In the measurement, a single addition of inhibitor is added to reaction centers before a standard binding titration is made with the active quinone. At high concentration, the functional quinone replaces the inhibitor at the active quinone site. The equations governing the interaction of reaction centers and action of inhibitor quinones are:

$$RC_{Free} + Q_{Free} \rightarrow RC \cdot Q$$

$$RC_{Free} + Inhibitor_{Free} \rightarrow RC \cdot Inhibitor$$

$$Inhibitor_{Total} = Inhibitor_{Free} + RC \cdot Inhibitor$$

$$RC_{Total} = RC_{Free} + RC \cdot Q + RC \cdot Inhibitor$$

$$K_d = \frac{([RC_{Total}] - [RC \cdot Q] - [RC \cdot Inhibitor]) \cdot ([Q_{Total}] - [RC \cdot Q])}{[RC \cdot Q]} \quad (2.9)$$

$$K_I = \frac{([RC_{Total}] - [RC \cdot Q] - [RC \cdot Inhibitor]) \cdot ([Inhibitor_{Total}] - [RC \cdot Inhibitor])}{[RC \cdot Inhibitor]} \quad (2.10)$$

Where $Inhibitor_{Free}$ is the unassociated inhibitor quinone, $Inhibitor_{Total}$ is the total added inhibitor quinone. $RC \cdot Inhibitor$ refers to the RCs bound with the Inhibitor quinone. $RC \cdot Q$ refers to the RCs bound with functional quinone. K_d is the dissociation constant of the active quinone, K_I is the dissociation constant of the inhibitor quinone.

In RCs with UQ_{10} in the Q_A site, the ability of a compound to competitively inhibit binding of UQ_1 at the Q_B site provides a measure its affinity for the site. The binding affinity of the inhibitor quinone is independent of its ability to function in the Q_B site. RCs with a single quinone in the Q_A site were prepared by adding UQ-10 to fully quinone removed RCs. These had 100% of the Q_A site occupied and 10-15% of the Q_B site occupied by the native UQ_{10}. The initial $P^+UQ_B^-$ is subtracted from the kinetic trace to account for the pre-existing UQ_{10} at Q_B. Reconstitution of Q_B with UQ_1 was monitored by the presence of a slower phase of the charge recombination kinetics. To determine the affinity of a non-native inhibitor quinone, a single addition of inhibitor XQ was made prior to the UQ_1 titration and a new apparent K_d^{app} measured. The dissociation constant of inhibitor is obtained assuming

$$Inhibitor_{Total} = Inhibitor_{Free}$$

$$K_i = [Inhibitor]/(k_d^{App} / k_d - 1) \quad (2.11)$$

This is appropriate because $Inhibitor_{Total}$ >> RC_{Total}, so the amount of RC·Inhibor is negligible. This method can also be used for measuring the K_d for a functional quinone with a very tight binding affinity as long as the activity of the active and inhibitor quinones can be distinguished (Figure 2.4b).

2.9 Determination of Thermodynamics from Thermal Back Reaction

The observed charge recombination kinetics can monitor the equilibrium reaction free energy of several reactions (Li, Takahashi et al. 2000). Starting in the $P^+Q_A^-$ or $P^+Q_B^-$ state, the system can return to the ground state through two paths: a direct route and via a thermal back reaction route. The rate of charge recombination by the thermal pathway (k_{AHP}) is proportional to the equilibrium constant between $P^+Q_A^-$ and P^+H^- (K_{eq}) and the charge recombination rate of P^+H^- (k_{HP}):

$$k_{AHP} = k_{HP} /(K_{eq}^{HA} + 1)$$

Thus, observed rate of charge recombination is

$$k^{obs} = k_{direct} + k_{thermal} = k_{direct} + k_{direct} /(K_{eq} + 1) \quad (2.12a)$$

k_{direct} is the direct tunneling rate that is temperature independent. This is k_{AP} starting from $P^+Q_A^-$ and k_{BP} starting from $P^+Q_B^-$ (Figure 2.5). $k_{thermal}$ is the thermal back reaction rate. The thermal route for Q_A recombination is via reformation of P^+H^- which decays at k_{direct} = k_{HP}. Similarly for Q_B recombination the thermal route is via $P^+Q_A^-$ that decays at k_{AP}. The amount of reaction via the thermal route is controlled by the equilibrium constant for charge recombination. Thus, free energy gap between $P^+Q_A^-$ and P^+H^- (ΔG^o_{HA}) controls the concentration of P^+H^-.

$$k_{AP}^{obs} = k_{AP} + k_{AHP}$$

$$= k_{AP} + k_{HP} /(K_{AH} + 1)$$

$$= k_{AP} + k_{HP} \cdot \exp(-\Delta G^{o}_{HA} / k_B T) \quad (2.11b)$$

Likewise ΔG^{o}_{AB} controls the amount of $P^{+}Q_A^{-}$ formed from $P^{+}Q_B^{-}$.

$$k^{obs}_{BP} = k_{BP} + k_{BAP}$$

$$= k_{BP} + k_{AP} /(K^{AB}_{eq} + 1)$$

$$= k_{BP} + k_{AP} \cdot \exp(-\Delta G^{o}_{AB} / k_B T) \quad (2.12c)$$

2.10 Low Temperature Measurements

The low-temperature measurements were carried out in a closed cycle helium cryostat system (APD cryogenics, CSW202A) with a programmable temperature controller. The temperature resolution is 0.1K and controllability is 0.4K. The light path of the optical cuvette is 1mm. The optical set-up is similar to that shown in Figure 2.1 except the actinic light and measuring light

The reaction centers in 10 mM Tris buffer is mixed with 2 volumes of glycerol. The final concentration of reaction center is 3-4μM for single-wavelength kinetics measurements. For the UQ_B reconstitution, UQ/RC was added 15-20.

The setup is kept under vacuum to keep the low temperature while doing experiment. For best pumping results, the system is dehumidified first. Helium gas in the closed cycle refrigerator is used to cool the system.

The measurements start after temperature reaches the desired one. The results from 10 flashes at 3 minutes interval were averaged. The measuring light is turned off between flashes.

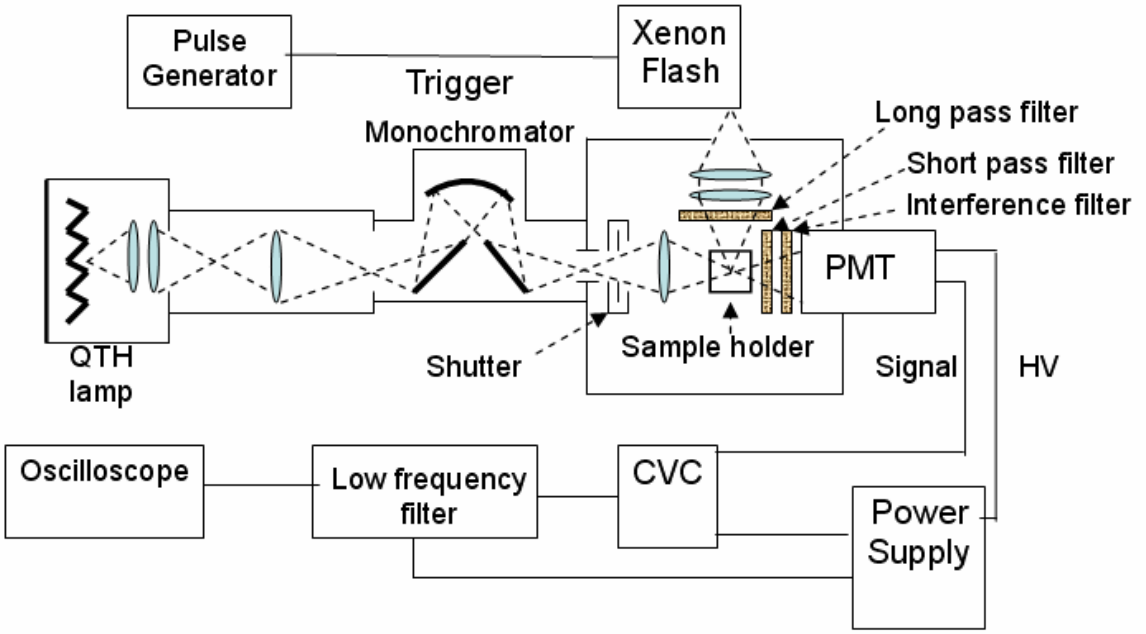

Figure 2.1 Setup for measurement of flash induced absorption change at a single wavelength.

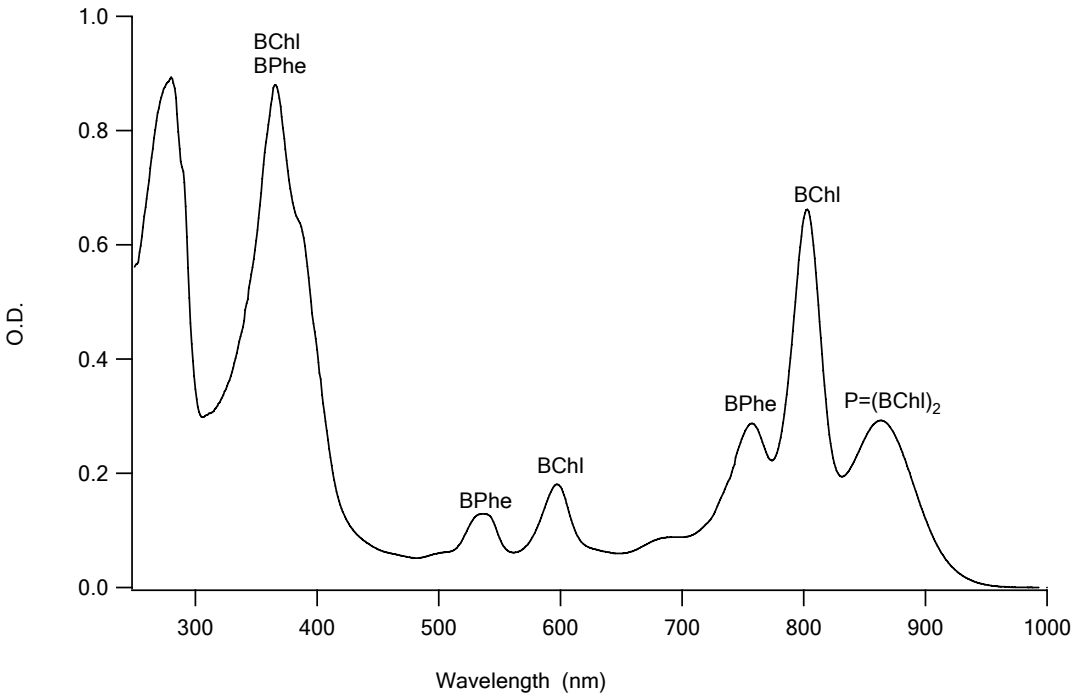

Figure 2.2 Absorption spectra of reaction centers isolated from the purple bacteria *Rb. Sphaeroides*. BChl: bacteriochlorophyll; BPh: bacteriopheophytin; P: the dimer of bacteriochlorophyll.

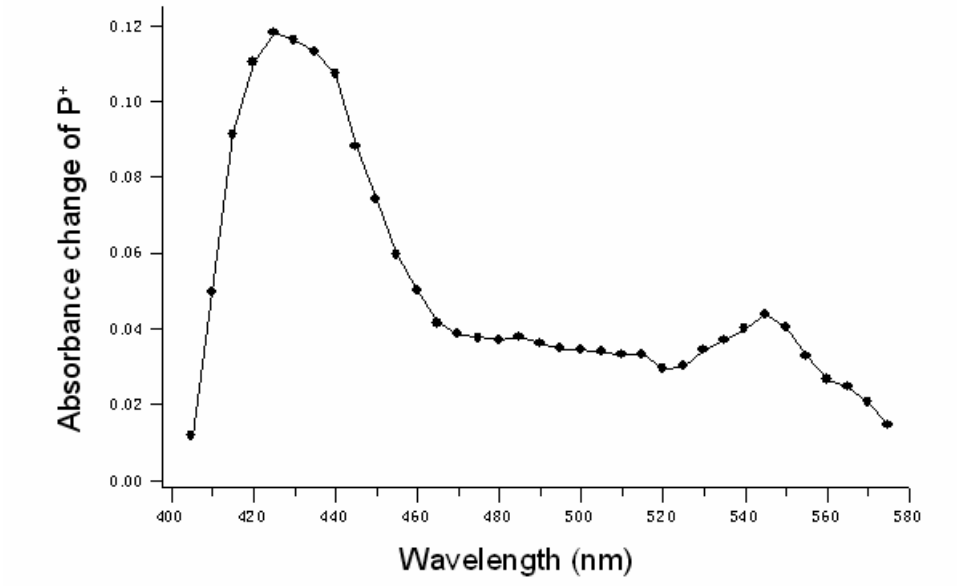

Figure 2.3 The spectra of light-induced absorbance changes of reaction centers from *Rb. Sphaeroides*. The absorbance change is positive in the visible light range. The absorption changes are mostly due to the oxidized special pair P^+, which has a maximum at 430 nm.

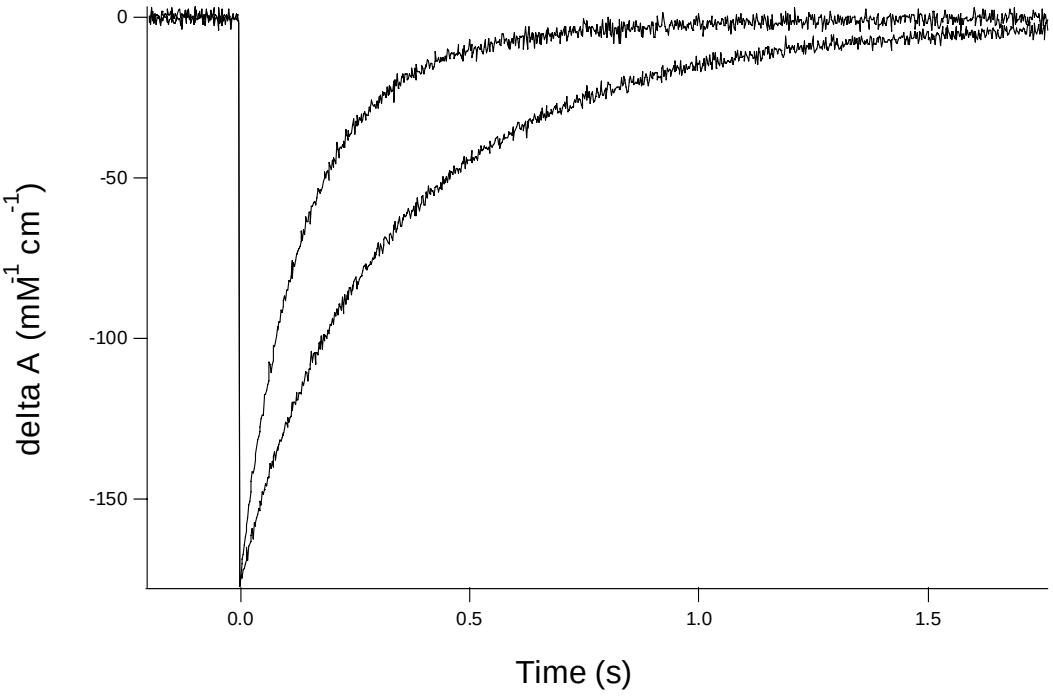

Figure 2.4 The flash-induced absorbance changes for P^+ to P at 430 nm. The upper curve is Ubiquinone at Q_A site with inhibitor o-phenanthrone bound to the Q_B site. The reaction rate k_{AP}^{obs} is 10/s, the half time is 70ms. The lower trace is for RCs with saturated Ubiquinone at both sites. The reaction rate k_{AP}^{obs} is 0.87 s^{-1}, the half time is 795 ms. The measurement is taken with 2.3 μM RC, 10mM Tris, pH = 7.85 at 298 ± 2K.

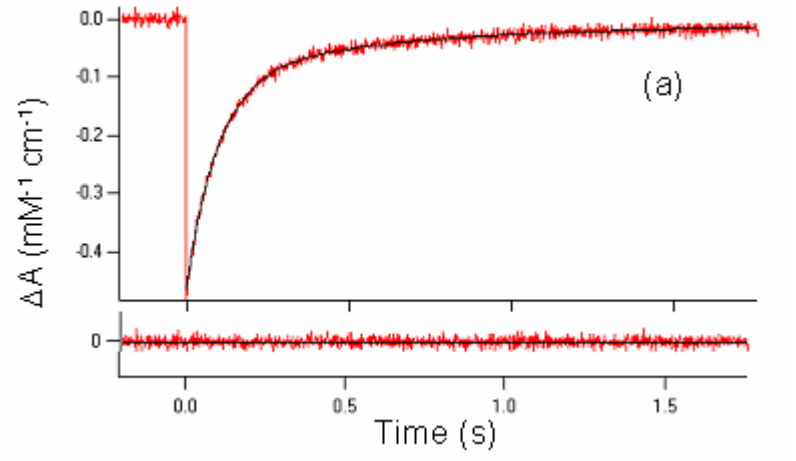

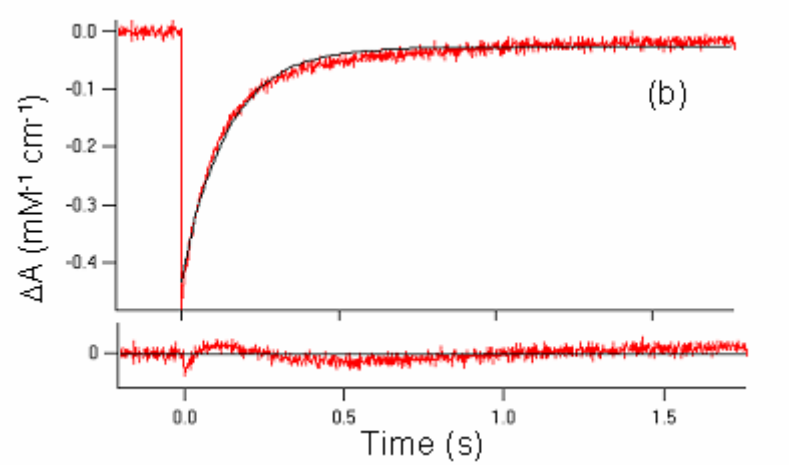

Figure 2.5 The data analysis of the flash-induced absorbance change for RCs with 100% UQ_A and 10-15% UQ_B. The red curve is the measured flash-induced absorption change. The black curve is the theoretical curve. The double-exponential is better fitting for this mixed population of RCs. The residual error is also shown. a) Double-exponential plus a constant: $A(t) = A_0 + A_{fast} \exp(-t / k_{fast}) + A_{slow} \exp(-t / k_{slow})$. A is the absorption change, k is the rate constant. A_0 is constant. The fast phase shows RCs where the electron returns

from $P^+Q_A^-$ state: A_{fast} = 76%, k_{fast} = 10.5s^{-1}; the slow phase represents the RCs where the electron return from $P^+Q_B^-$ state, A_{slow} = 22%, k_{slow} = 1.8s^{-1}. A_0 is 2% b) Single-exponential plus a constant fit to the kinetics: $A(t) = A_0 + A_{sin\,gle} \exp(-t / k_{sin\,gle})$. A_0 = 6%; A_{single} = 94%, k_{single} = 6.9 s^{-1}.

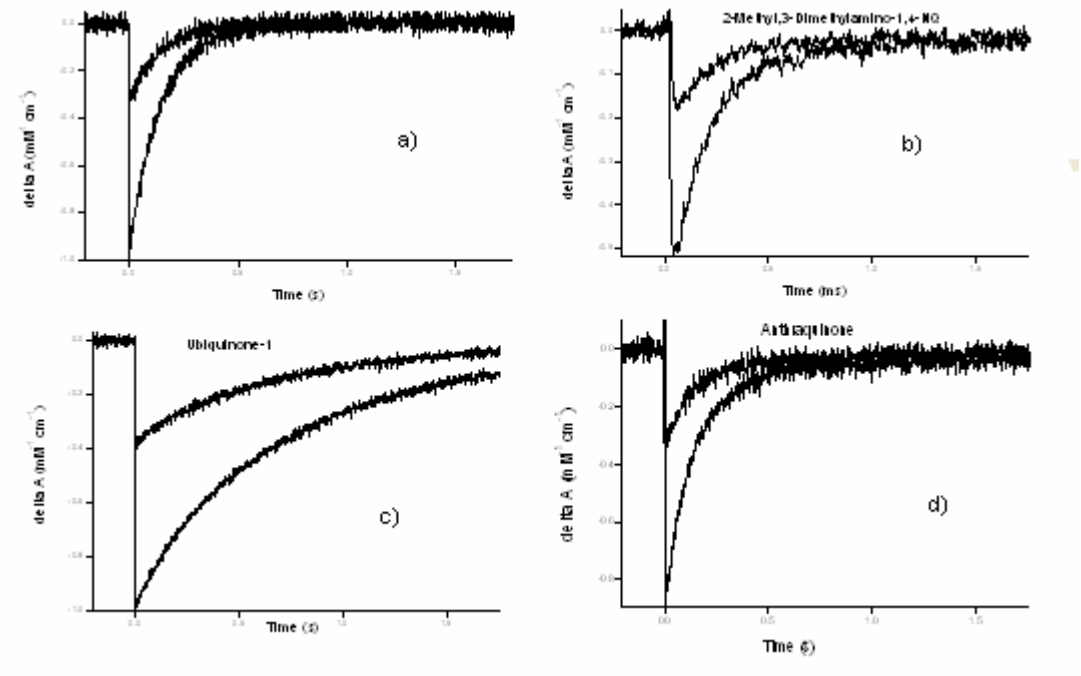

Figure 2.6: The flash-induced absorbance change for different quinones at the QA site at both 430 nm (bottom) and 550 nm (top). a) Ubiquinone-1 at Q_A. At 430nm, $k_{\sin gle}^{obs}$ =7.0s^{-1}, A_{single} = 99%; at 550nm, $k_{\sin gle}^{obs}$ = 6.6s^{-1}, A_{single}=97%. b) dMA-NQ at Q_A. At 430nm, $k_{\sin gle}^{obs}$ =5100s^{-1}, A_{single}=95%; at 550nm, $k_{\sin gle}^{obs}$ =4500s^{-1}, A_{single}=92%. c) UQ_A and UQ_B. At 430nm: k_{fast}^{obs} =10s^{-1}, A_{fast}=8%, k_{slow}^{obs} =1.36s^{-1}, A_{fast} = 92%; at 550nm: k_{fast}^{obs} =10s^{-1}, A_{fast} = 8%, k_{slow}^{obs} =1.36s^{-1}, A_{slow}=92%. d) Anthraquinone at Q_A. At 430nm, $k_{\sin gle}^{obs}$ =152s^{-1}, A_{single}=88%; at 550nm, $k_{\sin gle}^{obs}$ =155s^{-1}, A_{single}=84%. The maximum absorbance change at 430 nm is larger than those at 550 nm (Figure 2.3).

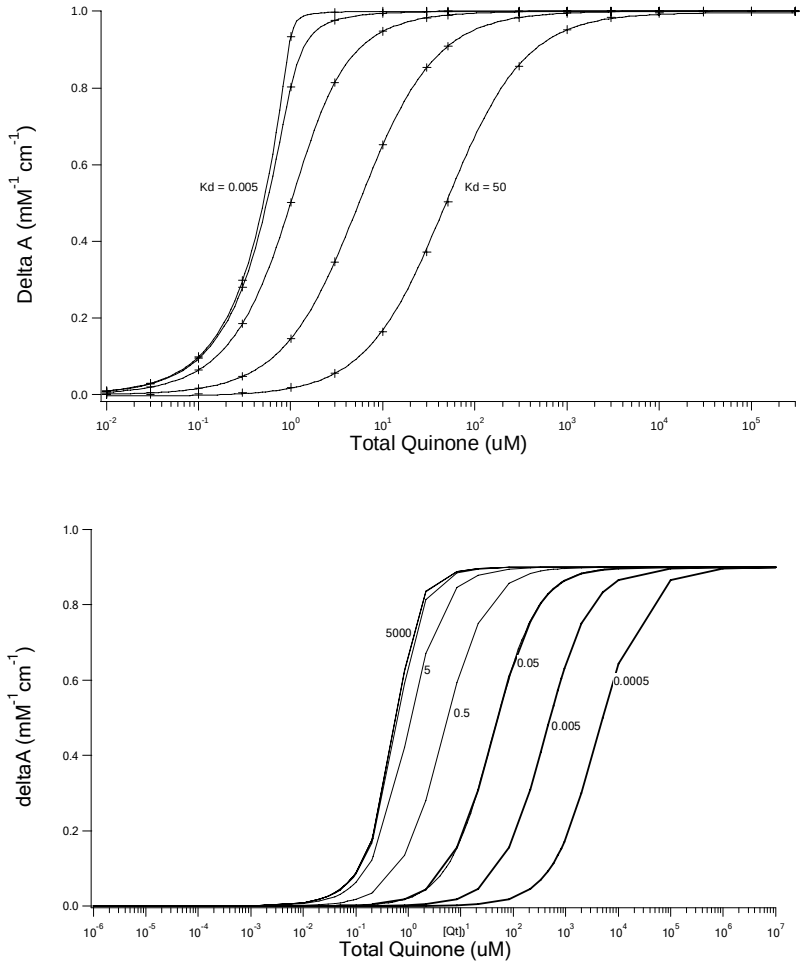

Figure 2.7 Theoretical of binding titration. a) The titration binding curve for functional quinone. [RC_{Total}] is 1μM. b) Competitive inhibition with non-functional quinone. [RC_{Total}] = 1μM, [$Inhibitor_{Total}$] = 20μM. K_d of functional Ubiquinone-1 is 0.1uM. The binding curve shifts toward the right with higher apparent dissociation constant K_d^{app} as the affinity of the inhibitor quinone increases (smaller K_I).

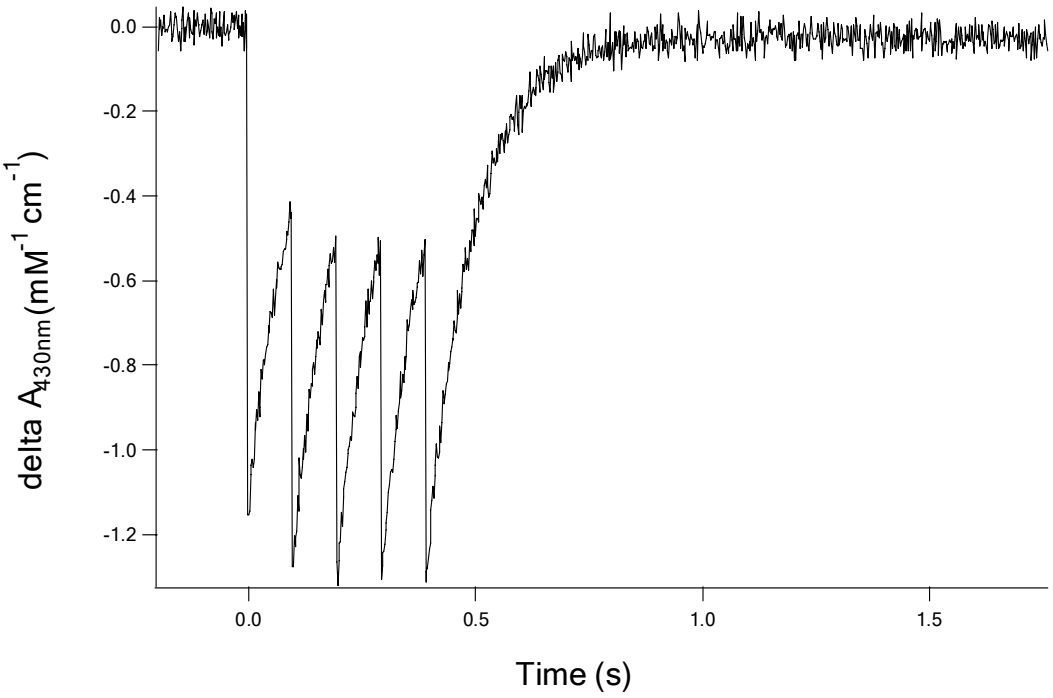

Figure 2.8 Charge recombination monitored by the absorbance change at 430nm as a function of time. 5μM RCs with UQ-1 at the Q_A site, 10mM Tris, 0.05% LDAO, pH=7.85 at 298±2K. Time interval between two flashes is 100ms. Not all RCs in the ground are excited with charge separation. Only 90% of the RCs are excited by the first flash compared with the saturating amount found after the 5th flash. Leaving 90% $P^+Q_A^-$ and 10% PQ_A. Before the charge recombination happens ($\tau_{1/2}$ is 70ms), the second flash excites 90% of the remaining PQ_A. After the second flash, the absorbance change of P^+ is mixed with $P^+Q_A^-$ from both flashes. After more flashes, 100% of the reaction centers are with $P^+Q_A^-$ state. This shows the light saturation of the flash lamp is 90%.

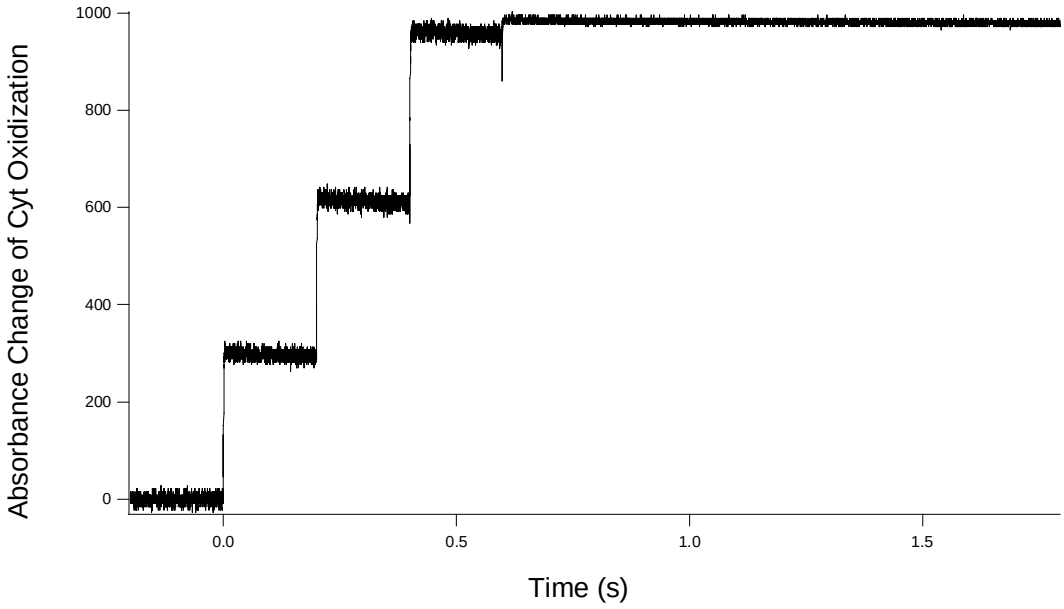

Figure 2.9 Cytochrome c oxidization following 5 flashes. [RC] = 5μM, reduced cytochrome c 200μM. The time interval between two flashes is 200 ms. The first flash: the charge separation forms $P^+Q_A^-Q_B$. At the same time, reduced cytochrome c is oxidized and P^+ is reduced ($Cyt^1_{red} + P^+Q_A^-Q_B \rightarrow Cyt^1_{oxd} + PQ_A^-Q_B$), with a half time of 100μs. The first step reflects the absorbance changes of oxidized cytochrome c Cyt^1_{oxd} and semiquinone Q_A^-. Before the 2nd flash occurs, the electron transfers from Q_A^- to Q_B: $PQ_A^-Q_B \rightarrow PQ_AQ_B^-$, in 100~200μs. The second flash forms $P^+Q_A^-Q_B^-$, and another reduced cytochrome c donates one electron to P^+: $Cyt^2_{red} + Cyt^1_{oxd} + P^+Q_A^-Q_B \rightarrow Cyt^1_{oxd} + Cyt^2_{oxd} + PQ_A^-Q_B$. As described in the text, with 2 quinones in the reaction centers 3 cytochrome c are oxidized.

References

Goldsmith, J. O. and S. G. Boxer (1996). "Rapid isolation of bacteria photosynthetic reaction centers with an engineered poly-histidine tag." Biochim. Biophys. Acta 1276: 171-175.

Graige, M. S., G. Feher, et al. (1998). "Conformational gating of the electron transfer reaction Q_A-Q_B Q_AQ_B- in bacterial reaction centers of *Rhodobacter sphaeroides* determined by a driving force assay." Proc. Natl. Acad. Sci. USA 95: 11679-11684.

Gunner, M. R. and P. L. Dutton (1989). "Temperature and -ΔG^o dependence of the electron transfer from BPh- to Q_A in reaction center protein from *Rhodobacter sphaeroides* with different quinones as Q_A." J. Am. Chem. Soc. 111: 3400-3412.

Kleinfeld, D., M. Y. Okamura, et al. (1984). "Electron transfer in reaction centers of *Rhodopseudomonas sphaeroides:* I. Determination of the charge recombination pathway of $D^+Q_AQ_B$- and free energy and kinetic relations between Q_A-Q_B and Q_AQ_B-." Biochim. Biophys. Acta 766: 126-140.

Halsey, Y. D. and W. W. Parson (1974). "Identification of ubiquinone as the secondary electron acceptor in the photosynthetic apparatus of Chromatium vinosum." Biochim Biophys Acta 347(3): 404-16.

Li, J., E. Takahashi, et al. (2000). "-ΔG^o_{AB} and pH dependence on the electron transfer from P^+Q_A-Q_B to $P^+Q_AQ_B$- in *Rhodobacter sphaeroides* reaction centers." Biochemistry 39: 7445-7454.

Loach, P. A. and S. L. Sekura (1968). "Primary photochemistry and electron transport in *Rhodospirillum rubrum*." Biochemistry 7: 2642-2649.

McComb, J. C., R. R. Stein, et al. (1990). "Investigations on the influence of headgroup substitution and isoprene side-chain length in the function of primary and secondary quinones of bacterial reaction centers." Biochim. Biophys. Acta 1015: 156-171.

McPhalen, C. A. and M. N. James (1987). "Crystal and molecular structure of the serine proteinase inhibitor CI-$_2$ from barley seeds." Biochemistry 26: 261-269.

Okamura, M. Y., R. A. Isaacson, et al. (1975). "The primary acceptor in bacterial photosynthesis: Obligatory role of ubiquinone in photoactive reaction centers of *Rhodopseudomonas sphaeroides."* Proc. Natl. Acad. Sci. USA 72: 3492-3496.

Parson, W. W. (1969). "The reaction between primary and secondary electron acceptor in bacterial photosynthesis." Biochim. Biophys. Acta 189: 384-396.

Straley, S. C., W. W. Parson, et al. (1973). "Prigment content and molar extinction coefficients of photochemical reaction centers from *Rhodopseudomonas sphaeroides.*" Biochim. Biophys. Acta 305: 597-609.

Vermeglio, A. and R. K. Clayton (1977). "Kinetics of electron transfer between the primary and secondary electron acceptor in reaction centers from *Rhodoseudomonas sphaeroides."* Biochim. Biophys. Acta 461: 159-165.

Woodbury, N. W., W. W. Parson, et al. (1986). "Radical-pair energetics and decay mechanisms in reaction center containing anthraquinones or benzoquinones in place of ubiquinone." Biochim. Biophys. Acta. 851: 6-22.

Wraight, C. A. (1979). "Electron acceptors of bacterial photosynthetic reaction centers II. H+ binding coupled to secondary electron transfer in the quinone acceptor complex." Biochim. Biophys. Acta 548: 309-327.

Wraight, C. A. and R. K. Clayton (1973). "The absolute quantum efficiency of bacteriochlorophyll photoxidation in reaction centers." Biochim. Biophys. Acta 333: 246-260.

Xu, Q. and M. R. Gunner (2001). "Trapping conformational intermediate states in the reaction center protein from photosynthetic bacteria." Biochemistry 40: 3232-3241.

Affinity and Function of Non-native Quinones at the Q_B Site of Bacterial Photosynthetic Reaction Centers

3.1 Abstract

Type II reaction centers (RCs) have 2 quinones that serve as sequential electron acceptors following light activated electron transfer. The native quinone in the purple bacterial *Rb. sphaeroides* is Ubiquinone (UQ). Only UQ can reconstitute both Q_A and Q_B function in the same RCs (i.e. XQ_A and XQ_B). The quinone binding affinity at the Q_B site was found to be 10-20 times weaker than at the Q_A site for quinones as large as 2-methyl-1, 4-Naphthoquinone. However, with the addition of one more methyl group, 2, 3-dimethyl-1, 4-Naphthoquinone does not fit into the Q_B site. (3) With a low potential electron donor 2-Methyl, 3-dimethyl-1, 4-Naphthoquinone (dMA-NQ), electron transfer to 1, 4-Naphthoquinone (NQ) at the Q_B site can be seen and this reaction is characterized. (4) The temperature dependence of the back reaction with dMA-NQ as Q_A and NQ as Q_B, is used to determine an upper level for the energy of NQ_B.

3.2 Introduction

Quinones are redox active cofactors found in many transmembrane proteins that couple electron and protein transfer reactions including Photosystem I (Fromme, Jordan et al. 2001), Photosystem II (Rutherford and Krieger-Liszkay 2001), cytochrome bc_1 (Hunte, Palsdottir et al. 2003), and b_6f complexes (Kurisu, Zhang et al. 2003; Stroebel, Choquet et al. 2003; Cramer, Zhang et al. 2004). In the photosynthetic reaction center from *Rhodobacter sphaeroides*, the Q_A and Q_B sites bind Ubiquinone-10. The protein modulates their electrochemistry so they can play different roles. Q_A, the primary

electron quinone acceptor that is tightly bound so does not leave the protein and accepts only one electron. Q_B, the secondary electron acceptor is loosely bound to the protein. Q_B can be found in three relatively stable redox states: the neutral quinone, anionic semiquinone, and fully reduced and protonated dihydroquinone (Wraight 1979; Okamura, Paddock et al. 2000; Zhu and Gunner 2005). The anionic semiquinone binds more tightly to the Q_B site, while the quinone and dihydroquinone freely exchange with the quinone pool in the membrane (Diner, Schenck et al. 1984; Madeo and Gunner 2005). The protein modulates the in situ E_ms so electron transfer from Q_A and Q_B is favorable with a driving force (ΔG°_{AB}) of –60 meV (–1.4 kcal/mol) (pH 5-9) (Kleinfeld, Okamura et al. 1984; Shopes and Wraight 1987; Zhu and Gunner 2005).

While all other reaction center cofactors are shown in unique binding sites, Q_B has been found in at least two different positions in crystal structures (Stowell, McPhillips et al. 1997). The proximal binding site, assumed to be active, has the Ubiquinone head group closer to Q_A, while it is further out in the quinone tail channel in the inactive distal site.

The Q_A site can be functionally reconstituted with a large variety of non-native quinones (Okamura, Isaacson et al. 1975; Gunner, Tiede et al. 1982; Gunner, Braun et al. 1985) and quinoid compounds (Warncke and Dutton 1993). In contrast it appears that only Ubiquinone can reconstitute both Q_A and Q_B function with the same quinone (Baccarini-Melandri, Gabellini et al. 1980; Kleinfeld, Okamura et al. 1984; McComb, Stein et al. 1990). The ubiquinone activity is dependent only on the head group since 2,3-

dimethoxy, 5-methyl Benzoquinone (UQ_0), the tailless analogue of UQ_{10}, with its 50 carbon 10-isoprene unit tail will carry out the reaction (Baccarini-Melandri, Gabellini et al. 1980). However, many quinones (denoted XQ) when added to quinone depleted RCs show only Q_A activity, even at high concentrations. Thus, only UQ appears to be able to function in homologous electron transfer from UQ_A^- to UQ_B. There are a number of possible reasons for the lack of Q_B activity. The added quinone could not bind to the Q_B site or could bind only to the inactive distal site. Alternatively the rate of electron transfer from XQ_A^- to XQ_B (k_{AB}) could be too slow to compete with the charge recombination from XQ_A^- to P^+. Since the quantum yield, Φ_{AB}, is ~ 0, the charge recombination rate in the charge-separated state $P^+Q_A^-$ (k_{AP}) with many non-native quinones are significantly faster than found with UQ (Gunner 1991). The forward rate k_{AB} would have to remain proportionally faster then k_{AP} to see the electron on XQ_B (Eqn. 2.5). In addition, RCs must modulate the relative electrochemistry of Q_A and Q_B to ensure forward electron transfer is thermodynamically favorable (Zhu and Gunner 2005). Thus, with XQ_A^- to XQ_B the reaction ΔG^o_{AB} could be unfavorable. Previous work with RCs reconstituted with a mixture of two non-native quinones supports this mechanism (Giangiacomo and Dutton 1989). Thus, with an XQ_A with lower potential then the replacement YQ_B electron transfer from XQ_A^- to YQ_B can be seen.

In the work presented here the affinity of 9 quinones are compared at the Q_A and Q_B site. The Q_A site dissociation constant K_ds are determined by their ability to reconstitute function. The Q_B site K_ds are determined by their competitive inhibition of UQ_1 function at the Q_B site. In addition, several replacement quinones are studied with a

low potential at the Q_A site. Their functional and inhibitory K_ds are compared and the upper level of YQ_B redox potential is determined.

3.3 Materials and Methods

3.3.1 Quinone Synthesis

The quinone 2-methyl, 3-dimethylamino-1, 4-napthoquinone (dMA-NQ) was synthesized (Salmon-Chemin, Buisine et al. 2001). The starting material 2-methyl-1, 4-naphthoquinone (200mg, 1.16 mmol) was diluted in 0.5ml dichloromethane (DCM). Dimethylamine (5.82 mmol) was mixed with ethanol (2ml) in a 10 ml sealed round-bottom flask for 1 hour in an ice-water mixture at 0^oC. The Analytical silica gel TLC plate (Analtech, 250 microns) was used for monitoring the reaction (Figure 3.1). The mixture was purified by chromatography on a gravity eluting column matrix with 50:50 ethanol:mathanol followed by preparative TLC with a Silica Gel GF plate (Analtech, #02013, 1000 micros). The quinone purity was determined to be > 90% by NMR (Figure 3.2). Three quinones synthesized: 2-(CH-C=CH_2)-1,4-Naphthoquinone (Yadav, Reddy et al. 2003). 2-Decyl-1,4-Naphthoquinoe, and 2-Decyl-3-dimethylaminon-1,4-Naphthoquinoe. The quinone 2-Decyl, 3-dimethylamino-1, 4-Naphthoquinone (ddMA-NQ) was synthesized using the same method starting with 2-Decyl-1, 4-Naphthoquinone (Ashnagar, Bruce et al. 1983).

3.3.2 Determining the Occupancy of the Q_A and Q_B Sites.

RCs are prepared with no quinone bound. The reaction centers with only the Q_A site occupied is prepared by adding a single quinone, or reaction centers with Q_A and Q_B occupied are then prepared by adding mixtures of two quinones (XQ and YQ). At all

times quinones are assumed to be in equilibrium with the RCs so the occupancy of the Q_A and Q_B sites is given by the relative binding affinity (K_d) and concentration of each quinone and the reaction centers concentration. The occupancy of the binding sites is determined by the kinetics of the charge recombination. The $P^+Q_A^-$ or $P^+Q_B^-$ decay rates are different for each quinone. With two quinones XQ and YQ added, there are 7 possible RCs that can be divided into 4 classes: (1) Those with no Q_A in the RCs. Here the P^+H^- formed by a flash decays with a half time of 10 ns (Woodbury, Becker et al. 1985; Martin, Breton et al. 1986), so it is not seen by the optical measurements which starts at 50 μs. (Fig. 3.1). (2) Those with only a quinone occupying the Q_A site (XQ_A or YQ_A). Charge recombination from $P^+Q_A^-$ to PQ_A occurs as a nearly single exponential with a rate constant (k_{AP}^{obs}) which is characteristic of the quinone. The distinctive charge recombination rate constants for these RCs are determined in RCs with a subsaturating quantity of a single quinone added so that only the Q_A site is occupied. All quinones used here are active at the Q_A site. (3) Those with the same quinone occupying Q_A and Q_B sites (XQ_A: XQ_B or YQ_A: YQ_B). Forward electron transfer from XQ_A^- to XQ_B or YQ_A^- to YQ_B is determined from the appearance of a slower back reaction rate with larger concentrations of a single quinone added (k_{BP}^{obs}). This reaction is only found with ubiquinones at the Q_A and Q_B sites (Okamura, Isaacson et al. 1975); (Baccarini-Melandri, Gabellini et al. 1980; Kleinfeld, Okamura et al. 1984; McComb, Stein et al. 1990). (4) Those with different quinones occupying the Q_A site and Q_B sites (XQ_A: YQ_B or YQ_A: XQ_B). If electron transfer can occur from XQ_A^- to YQ_B, a distinctive slow phase in the back reaction kinetics is observed at appropriate concentrations of XQ and YQ.

With one quinone, a two-exponential fit of the charge recombination kinetics distinguishes between empty RC sites, XQ_A and XQ_A: XQ_B reaction centers. With two quinones, a three-exponential fitting determines the amount of empty RCs, XQ_A, YQ_A, or XQ_A: YQ_B RCs. In all cases any contribution from the residual UQ_{10} is subtracted from the signal. The rate constant for XQ_A and YQ_A is fixed at values determined with only one quinone added. There is no case where electron transfer from both XQ_A^- to YQ_B and from YQ_A^- to XQ_B is found. When there is no forward reaction from a given Q_A^- to a given Q_B, reaction centers with both Q_A and Q_B sites occupied show the back reaction characteristic of the quinone bound in the Q_A site.

3.3.3 Functional Quinone Binding at the Q_B Site.

Given the K_d of a quinone for the Q_A and Q_B binding sites, the distribution of quinone in either site can be determined at any concentration of quinone with Mathematica with equations 2.1 & 2.7 (Figure 3.3). With two quinones the assumptions are that: a) The system is at equilibrium; b) The quinone YQ will not bind to Q_B site with empty Q_A site (Li, Gilroy et al. 1998). Binding of XQ or YQ to Q_B does not depend on which quinone is at the Q_A site. As described above with 2 quinones added there are 7 types of reaction centers present ranging from those with no quinone, the 2 states with one quinone at Q_A and 4 with both quinone binding sites occupied. The aim is to determine the electron transfer activity from XQ_A to YQ_B. Addition, with more XQ_A or having an XQ with tighter binding to the Q_A site pushes the binding curve where YQ displaces XQ at the Q_A site to higher concentration, increasing the concentration of desired XQ_A: YQ_B reaction centers (shaded region in Figure 3.4). With the range of K_ds

and solubility of the quinones used as XQ_A and the affinity of YQ for the Q_A and Q_B sites, it is not possible to obtain 100% of the RCs in the desired configuration.

3.3.4 Determining Reaction Thermodynamics from Thermal Back Reaction

The observed charge recombination kinetics are used to monitor the equilibrium reaction free energy of several reaction centers reactions (Li, Takahashi et al. 2000). The thermal route Q_A charge recombination for low potential quinone is via reformation of P^+H^- which decays at $k_{direct} = k_{HP}$. Similarly for Q_B recombination the thermal route is via $P^+Q_A^-$ that decays at k_{AP}. The amount of reaction via the thermal route is controlled by the equilibrium constant for charge recombination. Thus, the free energy gap between $P^+Q_B^-$ and P^+H^- (ΔG^o_{HB}) controls the concentration of P^+H^-. In reaction centers where charge recombination from $P^+Q_A^-$ is via the thermal route, addition of $P^+Q_B^-$ does not change this. As long as the system remains at equilibrium, ΔG^o_{HB} controls the amount of $P^+Q_H^-$ formed from $P^+Q_B^-$:

$$\begin{aligned} k_{BP}^{obs} &= k_{BP} + k_{BHP} \\ &= k_{BP} + k_{HP}/(K_{BH} + 1) \\ &= k_{BP} + k_{HP} \cdot \exp(-\Delta G^o_{HB} / k_B T) \end{aligned} \qquad (3.1)$$

To estimate the reaction enthalpy and entropy formation of $P^+Q_A^-$ or $P^+Q_B^-$, the back reaction kinetics experiment are measured as a function of temperatures. k_{HP} occurs by direct tunneling mechanism, which is relatively temperature independent. The charge recombination through thermal back reaction $k_{thermal}$ such as k_{AHP} or k_{BAP} are temperature

dependent. Therefore, the thermodynamic parameters are obtained from the Van't Hoff plot of the thermal back reaction rate Log($k_{thermal} - k_{HP}$) vs. the reciprocal of temperature.

$$\log(k_{thermal} - k_{direct}) = \log k_{HP} + (\Delta S^o / 2.3k_B) - (\Delta H^o / 2.3k_B T) \quad (3.2)$$

Where k_B is the Boltzman constant, T is temperature.

3.4 Results and Discussion

3.4.1 Specificity of Quinones for the Q_A and Q_B Sites.

a) Quinone Binding Affinity for the Q_A Site.

The affinity of 10 quinones for the Q_A site was determined by the reconstitution of $P^+Q_A^-$ absorbance changes at 430 nm, near the peak of the P^+-P absorbance difference spectra. Without Q_A, the absorbance change of P^+ is not seen on flash activation because P^+H^- charge recombines with a $t_{1/2}$ of 10 ns, while the measurements are initiated ≈50 μs after the flash. The range of affinities varies by almost 10^5 fold from 1 nM to 90 μM (Table 1, Figure 3.5). As found previously the affinity increases as the number of rings increase from 1 (Benzoquinone, BQ) to 2 (Naphthoquinone, NQ) to 3 (Anthraquinone, AQ) (Warncke, Gunner et al. 1987). Thus, AQ binds 40 times (2.2 Kcal/mol) more tightly then BQ. Ortho-methyl groups also increase the affinity both on BQs and NQs.

Table I Characterization of replacement quinones at the Q_A site.

Quinone	Maximum Fraction of $[RC \cdot Q_A]$	Quantum Yield Φ_{HA}	k_{AB} (/s)	ΔG^o_{AH} (meV)
UQ-1	1	1.0	10	520#
DmBQ	0.4*	0.7	1.75	--
TmBQ	1	1.0	1.47	--
DQ	1	1.0*	10	550#
1,4-NQ	1	1.0*	7.8	540#
2mNQ	1	N/D	7.4	--
DmNQ	1	N/D	9.5	500#
DMA-NQ	0.5	0.66	3000	261
DdMA-NQ	0.4	N/D	550	300
AQ	0.9	0.89*	175	330

Notes: UQ_1:Ubiquinone-1(2,3-dimethoxy, 5-methyl benzoquinone); DmBQ: 2,6-Dimethyl-Benzoquione; TmBQ: TrimethylBenzoquinone; DQ: Duroquinone; NQ: 1,4-Naphthoquinone; 2mNQ: 2-Methyl-1,4-Naphthoquinone; DmNQ: 2,3-Dimethyl-1,4-Naphthoquinone; dMA-NQ: 2-methyl, 3-dimethylamino-1, 4-napthoquinone; ddMA-NQ: 2-Decyl-3-dimethylamino-1,4-Naphthoquinone; AQ: 9,10-Anthraquinone. All measurements made at 298±2 K, with 1 μM RCs, 10 mM Tris pH = 7.8; 0.005% LDAO. *Quantum yields determined by light saturation (Gunner and Dutton 1989). ΔG^o_{AH} determined from k_{AP} with Eqn. 2.5b assuming $k_{HP} = 7.7 \times 10^7$ s^{-1}; $k_{AP} = 9.3$ s^{-1}; ΔG^o_{AH} can

only determined by the rate of charge recombination when $k^{obs}_{AP} > k_{AP.}$ $^{\#}\Delta G°_{AH}$ obtained from delayed fluorescence (Woodbury, Parson et al. 1986).

The newly synthesized quinones 2-dimethyl-amino, 3-methyl-NQ (dMA-NQ) and 2-decyl, 3-dimethyl-amino-NQ (ddMA-NQ) has K_ds of 60 and 300 nM. Increasing the tail length on the dimethyl-amino NQ from a methyl to a decyl group weakens the affinity. It has been previously established that quinones with two tails bind weakly (Warncke, Gunner et al. 1994). It may be that both the decyl and bulky dimethyl-amino groups compete for the binding site in the ddMA-NQ.

Maximal charge separation when the site is fully saturated. The ΔA_{430} when Q_A site are saturated with UQ_1 is taken 100% of reaction centers that absorb a photon forming P^+. Four quinones show a smaller amplitude change (Table 1). AQ shows only 90% activity (Gunner and Dutton 1989). This is in agreement with earlier measurements which determined that the forward electron transfer rate from P^+H^- to Q_A slows as $-\Delta G^o_{AH}$ becomes less favorable (Gunner and Dutton 1989). Under these conditions the rate of charge recombination from H^- to P^+ become comparable to the rate of reduction of Q_A by H^-. The formation of the stable $P^+Q_A^-$ is now governed by equation 2.9. The quantum yield of dMA-NQ is measured by light saturation (Gunner and Dutton 1989). The measured quantum yield is 66%. This value is similar to that found for 2-dimethylamino-NQ and 1-amino-9,10-anthraquinone which have similar ΔG^o_{AH} (Gunner and Dutton 1989).

b) Quinone Binding affinity at the Q_B Site

The affinity of the non-native quinones for the Q_B site was determined by competitive inhibition. With only 1±0.2 UQ_{10}/RC the rate of charge recombination, the rate k_{AP} has been well characterized. At room temperature, the rate k_{AP} is fixed at 10 s^{-1}. Addition of UQ_1 yields a concentration dependent slow phase of the back reaction. The fixed back reaction rate from $P^+UQ_B^-$ is 1 s^{-1} (Figure 2.5). The K_d for UQ_1 is 1.8 μM, somewhat weaker then the 0.5 μM that has been found previously (McComb, Stein et al. 1990).

Non-native quinones added to RC with one UQ_{10}/RC act as competitive inhibitors of UQ_1 binding to the Q_B site. With a single addition of quinone (YQ) the back reaction rate k_{AP} is fixed. The $P^+UQ_B^-$ back reaction rate is treated as a free parameter. The rate found ranges from 1 to $2s^{-1}$, indicating that there is no additional electron transfer from UQ_{10} at the Q_A site to YQ_B. For most accurate measurements, 40 – 120 μM inhibitors was added, sufficient to change the K_d^{app} for UQ_1 by 2 to 10 fold. Comparison of the apparent K_d for UQ_1 with and without XQ added provides the K_i of YQ at the Q_B site. The results were analyzed with the appropriate, simplifying assumption that the concentration of quinone added (Q_{Total})is equal to the free quinone (Q_{free}) (Eqn. 2.11)

3.4.2 Relative Affinity of Quinones at Q_A and Q_B Sites.

The affinities of quinones at the Q_A and Q_B sites were compared (Figure 3.7). For all quinones except dMA-NQ, AQ and DmNQ the quinone affinity for the Q_B site is 12±3 fold weaker than for the Q_A site. This is good agreement with comparisons of the relative

affinities of ubiquinone with different tail lengths in detergent solution or hexane (McComb, Stein et al. 1990; Warncke, Gunner et al. 1994). However the 3 largest quinones dMA-NQ, AQ and DmNQ bind tightly to the Q_A site with K_ds < 200 nM, but they bind at least 2000 times more weakly to the Q_B site with K_ds > 100 μM. Thus, it appears that addition of a second ortho-methyl on the NQ ring exceeds the size of the binding site. This provides a explanation of how photosynthetic bacteria which make both UQ and 2-methyl-3-soprenyl-1,4-Naphthoquinone, Menaquinone (MQ) can segregate the correct quinone to each binding site. Thus, even in *Rb. sphaeroides*, an organism which does not make MQ, the 2,3-diMeNQ head group binds 30 fold tighter then UQ_1 to the Q_A site while at the Q_B site it binds more then >50 times weaker. The differential activity is such that dMA-NQ is found to displace UQ-10 from the Q_A site at concentrations that are insufficient for it to displace UQ_1 from the Q_B site.

Table II: Quinone binding affinity at Q_B site determined by competitive inhibition with UQ_1 in RCs with Q_A site with UQ_{10}. A single addition of YQ is added prior to the UQ_1 titration [DmBQ] = 42μM, [TmBQ] = 120μM, [DQ] = 48μM and [AQ] = 10μM. K_i is determined with Eqn. 2.11. Q_A K_ds from table 1. [RC] = 1μM, 10mM Tris, 0.005% LDAO, pH=7.8, T=298±2 K. UQ_1 was added to the Q_B site and generates [RC·UQ_B]. k_{BP}^{obs} of UQ_1 at Q_B is kept constant at 1.0/s.

Quinone	Q_A K_d (μM)	Q_B K_d (μM)	Maximum [RC·UQ_B]	k_{BP}^{obs} (s^{-1})	K_d at Q_B/K_d at Q_A
UQ-1	0.1	1.8±0.24*	>0.9	1.0	17
DmBQ	88	>500	0.8	--	6
TmBQ	16	>180	0.9	--	11
DQ	0.8	6.1±2.4	0.5	1.0-1.8	9
1,4-NQ	8	65±25	0.8	0.43-0.68*	8
2mNQ	1.4	20	0.6	--	14
AQ	0.2	160	>0.9	--	1000
dMA-NQ	0.06	>100	>0.9	--	1667
DmNQ	0.03	100	0.6	0.35-0.42*	3333

- [RC•UQ_B] is maximum fraction of functional UQ_1 bound at Q_B site.
- The binding affinities are measured by competition inhibitor with UQ_1 (Figure 3.6).
- *The binding affinity of UQ_1at the Q_B site was measured by direct titration methods.

3.4.3 Reconstitution of Q_B Activity

a) Characterizing the Low Potential Quinone in the Q_A Site

The rate of charge recombination and in situ Q_A E_m. The rate of charge recombination was measured at subsaturating quinone concentration when a negligible number of RCs have 2 quinones bound. As has been found before the methyl substituted BQs and the NQs show a rate slower than 10 s^{-1}, indicative of direct electron tunneling from Q_A^- to P^+. The faster rates found with AQ, dMA-NQ and ddMQ-NQ are used to determine the ΔG^o_{AH} for AQ and the dMA-NQ (Eqn. 2.5b). Thus, AQ is found to be 190 meV higher in energy then UQ in reasonable agreement with earlier results (Gunner and Dutton 1989; Xu and Gunner 2000). The 2-dimethyl-amino,3-methyl-NQ k_{AP} of 3000 s^{-1} (Figure 3.9) indicates that ΔG^o_{HA} is only 260 meV, placing the $P^+Q_A^-$ state 260 meV higher with the replacement that found with UQ at the Q_A site.

The thermal back reaction. To ensure that the fast back reaction represents charge recombination via the thermal back reaction via P^+H^- the ΔH^o and ΔS^o was determined for the dMA-NQ between 277K and 303K (Xu and Gunner 2000). The thermodynamic parameters are obtained by temperature dependence with Equation 3.2 (Figure 3.10). ΔH^o is –244 meV and $-T\Delta S^o$ is -19 meV at 298K. The enthalpy change, which is close to the reaction free energy dominates, and the entropy change is small as has been found previously (Xu and Gunner 2000). So the free energy change is weakly temperature-dependent. The free energy obtained here is 263 meV. Two methods are used to test the dMA-NQ energy level at Q_A site: one is thermal back reaction at room temperature

(Table I), the other is deduced from the enthalpy and entropy. The results from two methods match well.

b) Quinone Mixture to Reconstitute the Functional Q_B.

As has been shown previously (Giangiacomo and Dutton 1989), the activity of a quinone in the Q_B site depends on the quinone at the Q_A site. Only UQ can reconstitute both Q_A and Q_B function in the same RCs (i.e. XQ_A to XQ_B). While the affinity for the Q_B site does depend on the tail length, the ability to reconstitute UQ_B function is not dependent on the tail (McComb, Stein et al. 1990; Warncke, Gunner et al. 1994). With all other quinones no slow phase of charge recombination is seen that would be indicative of the electron transfer forming $P^+Q_B^-$.

In Q_A removed RCs the ability of the different quinones to support electron transfer from XQ_A to XQ_B was determined by monitoring the back reaction rate as a function of quinone concentration. As quinones are added to the empty Q_A site the amplitude of the $P^+Q_A^-$ signal increases. However, there is no change in electron transfer rate with quinone concentration for any of the quinones except UQ_1 (Figure 3.8b). Thus, there is no significant formation of YQ_B^- unless the quinone added to replace Q_A and Q_B is a Ubiquinone.

3.4.4 Determining of Functional Q_A to Q_B Activity with a Low Potential Quinone at the Q_A Site.

Functional XQ_A^- to YQ_B electron transfer has been found previously to require a low potential XQ_A and higher potential YQ_B and the study here confirms this conclusion

(Giangiacomo and Dutton 1989). Thus, a mixture of the low potential dMA-NQ and NQ does show charge recombination phases indicative of electron transfer to Q_B. The concentration dependence of the amplitude of the 3 phases of charge recombination was studied as a function of NQ concentration with 2μM dMA-NQ. With only the dMA-NQ the system returns to the ground state in a single, fast exponential. With increasing concentration of NQ, a new slow phase of charge recombination indicative of dMA-NQ_A: NQ_B RCs is seen, which is not found with either dMA-NQ or NQ alone (Figure 3.11). As more NQ is added it displaces dMA-NQ_A site and NQ_A back reaction kinetics are found. Thus, given the 6 possible RCs with one or two quinones bound there are three distinct kinetic phases seen: dMA-NQ_A only at low NQ concentration (dMA-NQ_A), NQ_A only (NQ_A) at high NQ concentration and dMA-NQ_A: NQ_B (dMA-NQ_A:NQ_B). No phase suggesting electron transfer from NQ_A^- to NQ_B (Figure 3.8b) or from NQ_A to a lower potential dMA-NQ_B is seen.

The kinetic phase indicative of dMA-NQ_A: NQ_B is formed in only ≈50% of the RCs (or of the RCs that form $P^+Q_A^-$). This low yield is a result of the relative rates of several competing electron transfer reactions in the RCs as well as the relative affinity of dMA-NQ and NQ for the two binding sites. The quinones compete for both binding sites. The relative K_ds of dMA-NQ and NQ for the Q_A site and the maximum amount of added dMA-NQ determine the final amount of active hybrid RCs (Figure 3.4). The dMA-NQ has been shown to be a very poor competitor for the Q_B site. With a K_d >100 μM, the 2 μM added can not significantly displace NQ_B. However, as more NQ is added to the binding site it displaces the dMA-NQ from the Q_A site as is found from the appearance of

a back reaction with a time constant characteristic of NQ_A. With more dMA-NQ at Q_A site, more 1,4-NQ is needed to compete at Q_A site. The dissociation constant of NQ at Q_B site will not be influenced (Figure 3.4). The solubility limit for the NQ in ethanol is ~26mM, beyond 1mM particles of 1,4-NQ scatters the light and weaks the signal. The concentration of 1,4-NQ with RCs kept below 1mM. The dMA-NQ is controlled around 2μM for 1μM RCs.

The rate k_{AB} for electron transfer from low potential quinone at the Q_A site to non-native quinone at the Q_B site can be derived by the quantum yield of $P^+Q_B^-$ (Eqn. 2.5). The total amplitude of RCs that shows the absorbance change of P^+ following a flash is A_{XQ} +A_{YQ} where A_{XQ} and A_{YQ} are the apparent amplitude for $P^+XQ_A^-$ and $P^+YQ_A^-$. The quantum yield for reduction of the low potential dMA-NQ_A is only 50% measured by the light saturation method, as the forward k_{HA} has slowed in these RCs and can no longer compete with k_{HP} (Gunner and Dutton 1989). Thus, a significant fraction of the RCs return to the ground state and have no opportunity to form a reduced Q_B. The electron at $P^+Q_A^-$ can transfer to the functional NQ at Q_B site. The second competition is between forward electron from $P^+Q_A^-$ transfer to Q_B (k_{AB}) and return to the ground state at k_{AP}. In UQ_A:UQ_B RCs, the forward rate is 100μs (Kleinfeld, Okamura et al. 1984; Mancino, Dean et al. 1984; Tiede, Vazquez et al. 1996). The quantum yield of $P^+Q_B^-$ can be derived by fitting the fraction of slow back reaction as a function of YQ added. The fraction forward reaction is treated as a free parameter when fitting. The maximum fraction of electron transfer between dMA-NQ_A to NQ_B is around 40% (Figure 3.11). Because the thermal back reaction rate k_{AP} from low potential dMA-NQ is around 3000/s,

the electron transfer rate k_{AB} between dMA-NQ at Q_A and NQ at Q_B, estimated by Eqn. 2.5, to be 2000/s (350μs).

3.4.5 Estimation of Energy Level for Non-native Q_Bs

For the native quinone at Q_A and Q_B sites, the charge recombination from $P^+Q_B^-$ goes via thermal reformation of $P^+Q_A^-$. The equilibrium between $P^+Q_A^-$ and $P^+Q_B^-$ can be estimated from k_{BP}^{obs} in a manner analogous to the use of the thermal back reaction to obtain the free energy of $P^+Q_A^-$ with low potential quinones (Eqn. 2.5b). The mixed RCs with dMA-NQ at Q_A and NQ at Q_B the slow phase of the back reaction rate is 0.68 s^{-1} (Figure 3.9). As this Q_A charge recombines via the P^+H^- state, the thermal back reaction path from $P^+Q_B^-$ must also use this route (Eqn. 3.2). The derived $-\Delta G^o_{HB}$ is 488 meV. The observed charge recombination rate from UQ_B k_{BP} progressively decreased from 293K to 225K, $\Delta H_{AB}^o = -150\pm11$ meV and $\Delta S_{AB}^o = -0.3\pm0.03$ meV (Mancino, Dean et al. 1984); (Schmid and Labahn 2000). The observed charge recombination rate is not linear with temperature as expected in a Van't Hoff plot (Figure 3.12). So the observed rate appears to be a combination of direct electron tunneling at k_{BP} and the thermal back reaction rate via $P^+Q_H^-$, at k_{BHP} (Figure 3.13). The direct tunneling rate, is weakly temperature-dependent (Schmid and Labahn 2000), while the thermal back reaction rate should be temperature-dependent. From the observed charge recombination rate k_{BP}^{obs}, the free energy, entropy and enthalpy change for either individual reaction cannot be estimated correctly. A reaction using 100% thermal back would be k_{BHP} required to estimate the thermodynamics parameters from k_{BHP}. The free energy $-\Delta G^o_{HB,}$ derived from k_{BP}^{obs} for the ΔG_{AB}, provides the upper limit for the energy of $P^+NQ_B^-$ (Figure 3.13).

Table III: Quinone's Em in the different environment.

	E_m in solution (DMF) (meV)	E_m in Q_A site (meV)	Estimated E_m in Q_B site (meV)
UQ	-600*	0	60
dMA-NQ	--	-260	--
NQ	-500	30 **	<-40
AQ	-750*	-160	--

*data from Woodbury, BBA 851 (1986) 6-22.

** data from Gunner, J. Am. Chem. Soc. 1989, 111, 3400-3412.

With 1,4-NQ at the Q_B site, the upper energy limit is estimated. The upper limit level of NQ_B is lower than Ubiquinone at both Q_A and Q_B sites. That explain why there is no electron transfer from Ubiquinone at the Q_A site to non-native quinone at the Q_B site. From Table III, the E_m difference between NQ and UQ in solution is around -100 meV. When the quinone is added to Q_A in RCs, the shift between NQ_A and UQ_A is 30 meV (Gunner and Dutton 1988). With a functional quinone at the Q_B site, the Em difference between UQ_B and NQ_B is approximately -100 meV. It indicates that reaction centers modulate the quinone energy at the different sites.

3.5 Conclusion

As found previously, it has been shown that the Q_A and Q_B sites cannot be reconstituted by quinones other than ubiquinone. The work presented here provides some reasons why. Two hypothesis were explored: one is that quinones that bind to the Q_A site do not bind to the Q_B site; the other is the quinones bind at the Q_B site, but the electron transfer between Q_A and Q_B is unfavorable because of how the reaction center modulates the E_m in the different sites.

The affinities of quinones at the Q_B site were determined by competitive inhibitor binding measurements. The binding affinity at the Q_A and Q_B sites was compared. For quinones up to the size of 2-methyl-napthoquinone the affinity at the Q_B site is approximately 13 times weaker then at the Q_A site. However, 2,3-dimethyl-napthoquinone binds >150 fold weaker at the Q_A site than it does at the Q_B site. The low affinity of the dimethyl quinone provides an explanation of how photosynthetic bacteria, which make both UQ and 2-methyl-3-isoprenyl-1,4-Naphthoquinone, Menaquinone (MQ), can segregate the correct quinone to each binding site. Thus, even in *Rb. sphaeroides*, an organism which does not make MQ, the 2,3-diMeNQ head group binds 30 fold tighter then UQ_1 to the Q_A site while at the Q_B site it binds more then >50 times weaker. Thus, some of the quinones, which do not function are too weakly bound while others are not.

1,4-Naphthaquinone was chosen of the quinones that have sufficient affinity that the Q_B site should be saturated at accessible quinone concentrations. In hybrid reaction

centers with a low potential dMA-NQ quinone at the Q_A electron transfer between low potential dMA-NQ_A and NQ_B was detected. Thus, electron transfer can be seen, but it requires added driving force. The upper limit level of the NQ_B E_m was found to be is lower than Ubiquinone at both Q_A and Q_B sites. Thus, electron transfer from Ubiquinone at the Q_A site to NQ at the Q_B site will be unfavorable, explaining why it is not found. The E_m difference between NQ and UQ in solution is different than the E_m shift at the Q_B site in reaction centers. This indicates that reaction centers affects the electrochemistry of each quinone at each binding site differently.

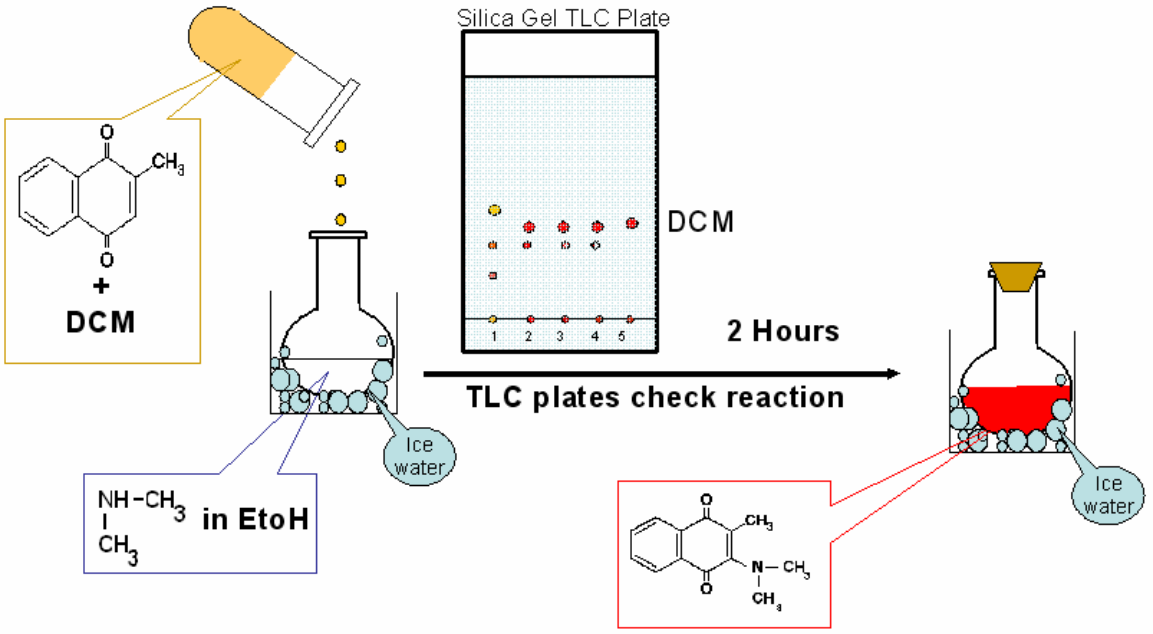

Figure 3.1: Synthesis of 2-Methyl, 3-Dimethylamino-1,4-Naphthoquinone. 1) The reactant DCM mixture only; 2) 2-methyl-1,4-Naphthoquinone dissolved in DCM; 3) DCM solution added to ethanol. 4) Reaction mixture sampled at different times. 5) At 2 hours, the reaction is complete.

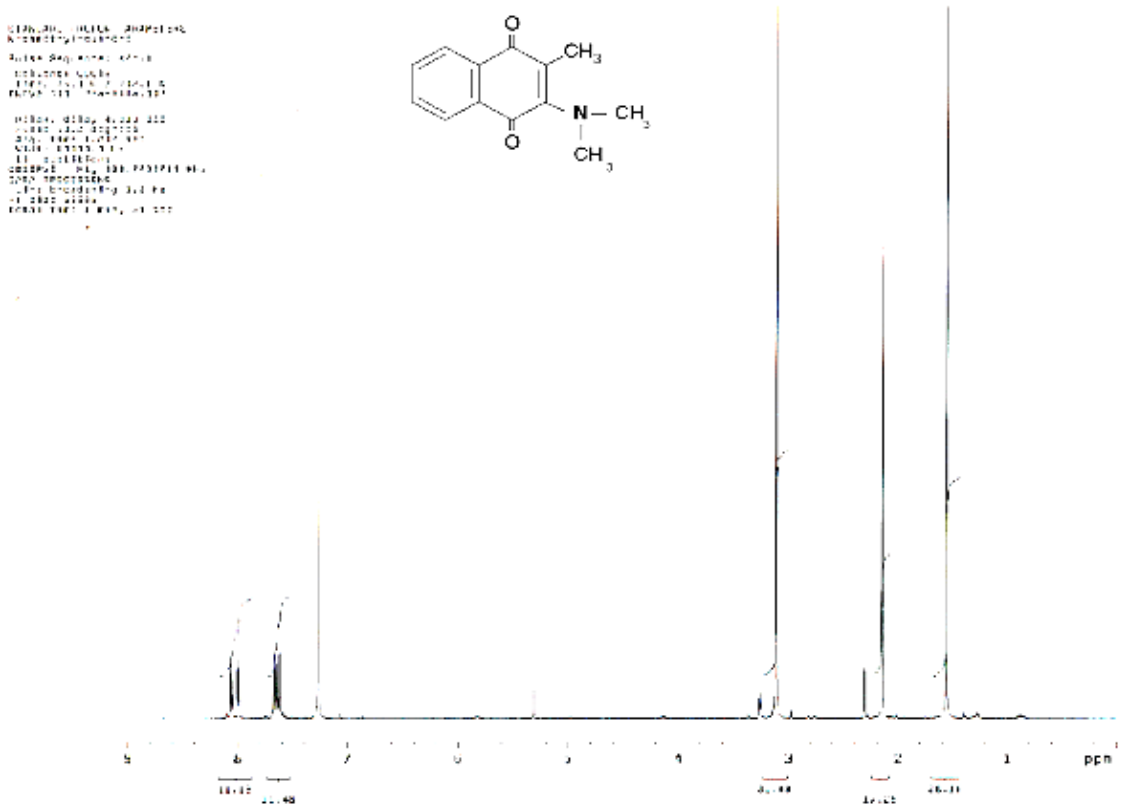

Figure 3.2 The NMR spectrum of 2-methyl,3-Dimethylamino-1,4-Naphthoquinone.

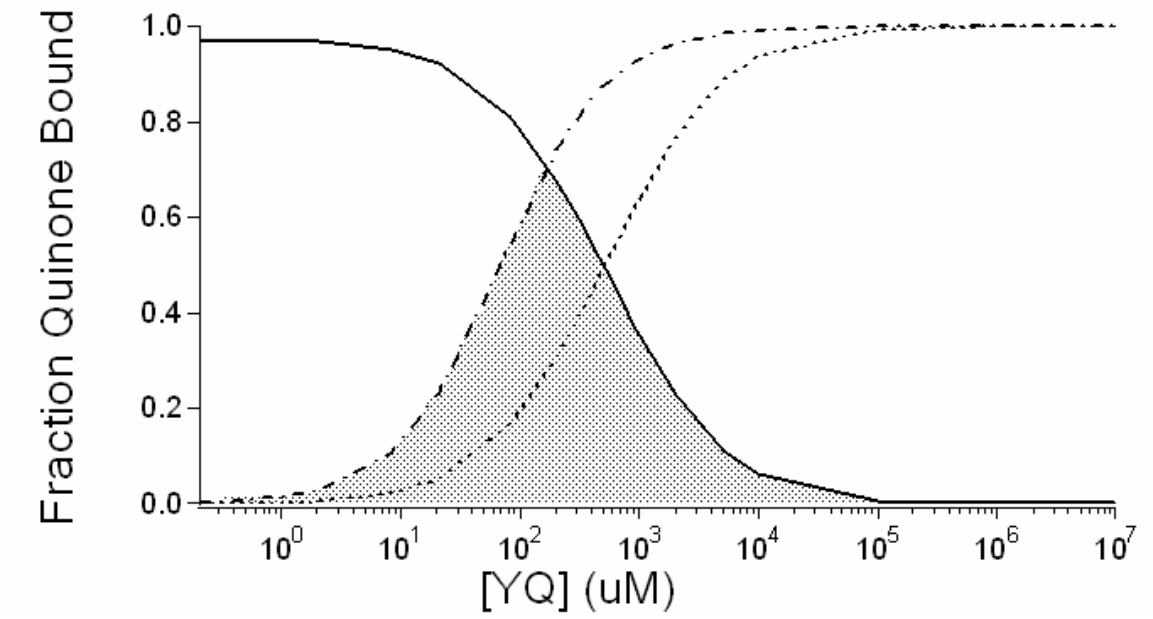

Figure 3.3: The occupancy of the Q_A and Q_B binding sites as a function of the concentration of YQ. In the model the RC concentration is 1μM and the XQ concentration is 2 μM and its K_d is 0.06 μM at the Q_A site and more than 1000μM at the Q_B site, for YQ the K_d at the Q_A site is 8 μM while it is 65 μM at the Q_B site. The solid line is the fraction of reaction centers with XQ_A (which may also have XQ_B); the dotted line represents the fraction with YQ_A (which may also have YQ_B or XQ_B); the dashed line shows the amount of YQ_B. The shaded region indicated the fraction of RCs with both XQ_A and YQ_B.

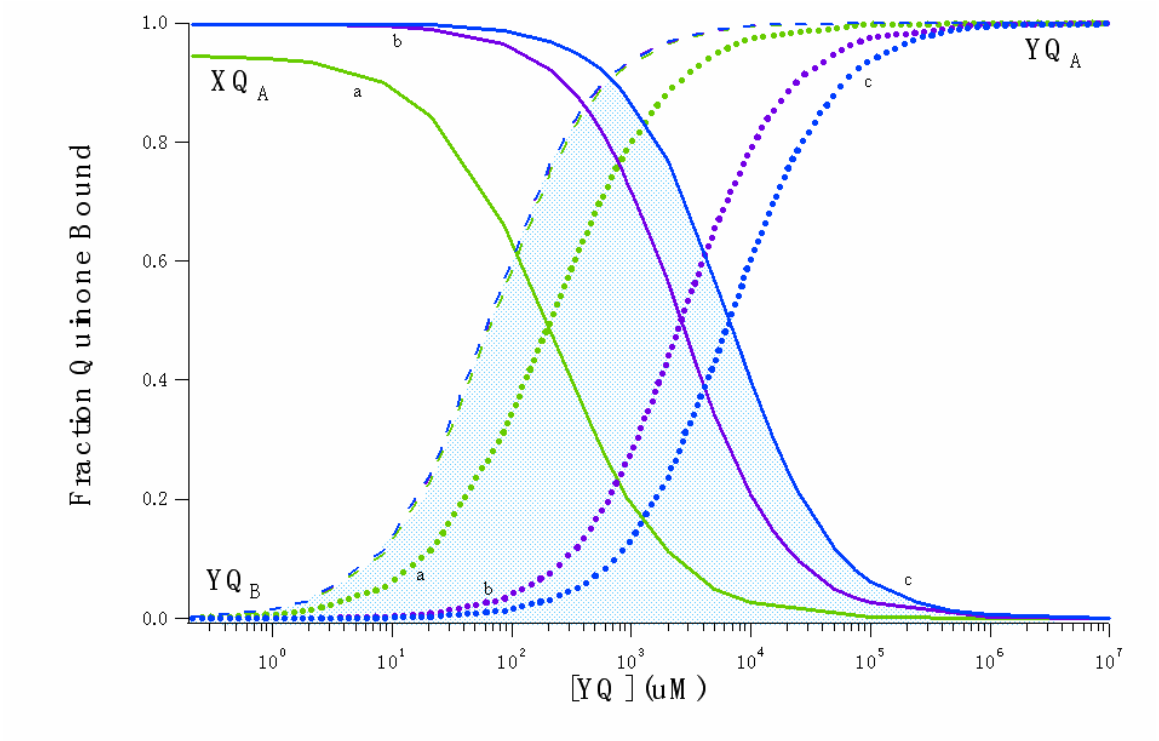

Figure 3.4 The theoretical simulation of a mixture of non-native quinones binding to RCs. The concentration of [XQ] are 2 μM, 20 μM and 50 μM, the binding affinity of XQ at Q_A is 0.06 μM. [RC]=1μM. The binding affinity of YQ at the Q_A site is 8μM and at Q_B is 65 μM. The solid lines refer to binding curves of XQ at the Q_A site, the dotted lines refer to binding curves of YQ at the Q_A site and the dashed lines refer to binding curves of YQ at the Q_B site. Green (a), purple (b) and blue (c) represent the binding curves with 2μM, 20 μM and 50 μM XQ, respectively. The area (the shaded region in the figure 3.3) between the solid XQ_A and dashed YQ_B binding curves indicates reaction centers with XQ_A and YQ_B. Both XQ_A and YQ_A binding curves shift to right and the apparent dissociation constant k_d^{app} of YQ_A increases, as the concentration of XQ is increases. Since YQ must competed with XQ to bind at the Q_A site. The binding curve of YQ_B (dashed line) does

not change with more XQ assuming XQ does not bind to the Q_B site. The desired XQ_A: YQ_B area increases with more XQ added.

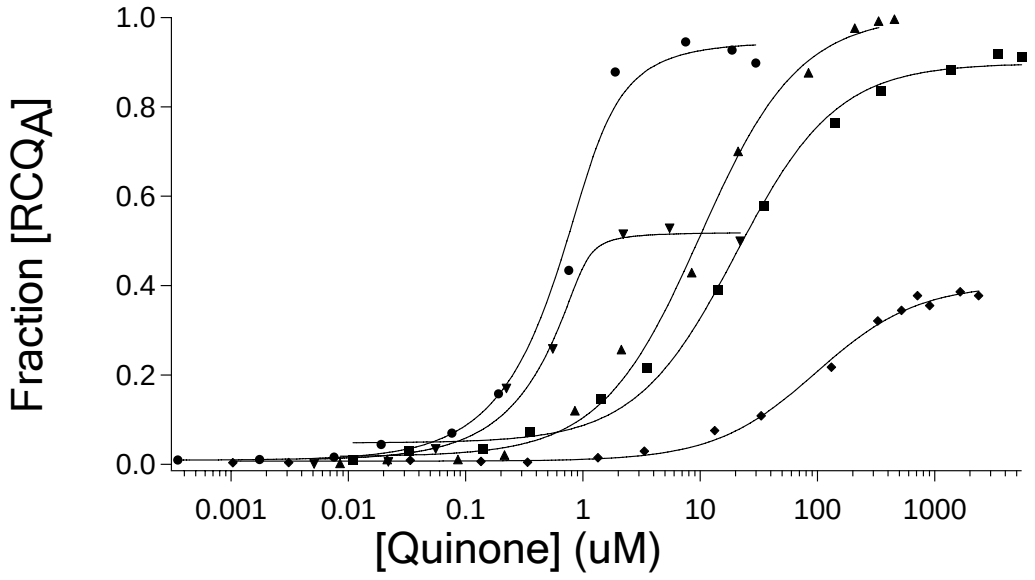

Figure 3.5. Q_A activity as a function of quinone concentration. The theoretical lines are the best fit to the data given Eqn. 2.3. Values for the K_d and maximum amplitude at saturation are given in Table 1. (●): 9, 10-AQ; (▼): dMA-NQ; (▲): 1,4-NQ; (♦) DmBQ; (■) TmBQ. Titration carried out with 1 μM RCs; 10mM Tris, pH=8.0 at T=298±2K.

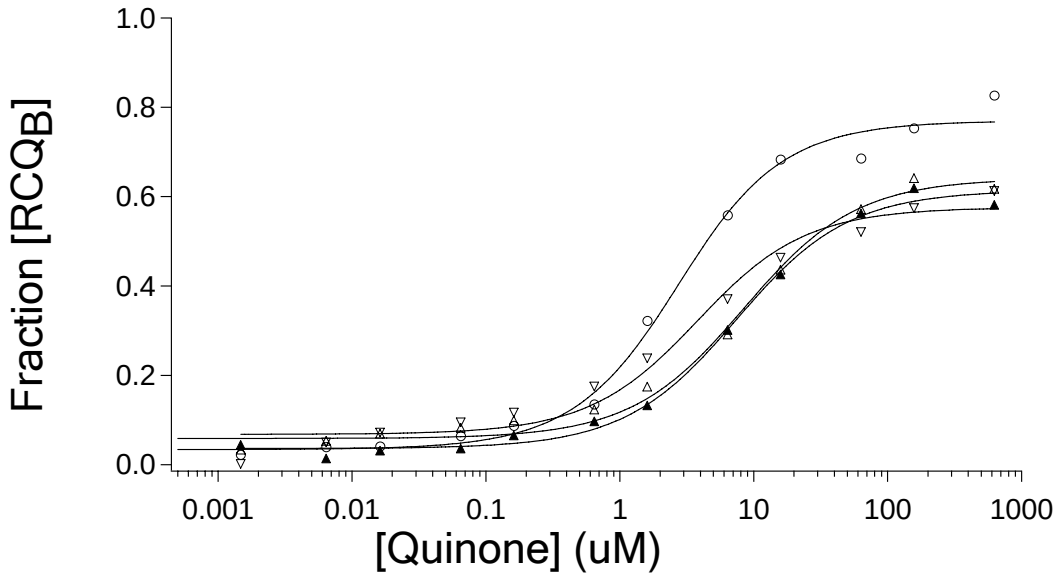

Figure 3.6 Reconstitution of QB function with UQ1 in the presence of non-native quinones as competitive inhibitors. (○): UQ_1 alone, Kd = 1.8 μM; (▲): NQ, 65 μM, K_d^{app} = 6.9 μM; (Δ): 2mNQ, 57 μM, K_d^{app} = 7.9 μM; (▽): DmNQ, 47 μM, K_d^{app} = 3.29 μM. [RC] =1 μM, 10mM Tris, pH=8.0, 0.005% LDAO at 298±2K, The Q_A site is saturated with UQ_{10}. The dissociation constant of inhibitor K_i derived from K_d^{app} and maximum fraction of $[RC{\cdot}UQ_B]$ at saturating UQ_1 are listed in Table II.

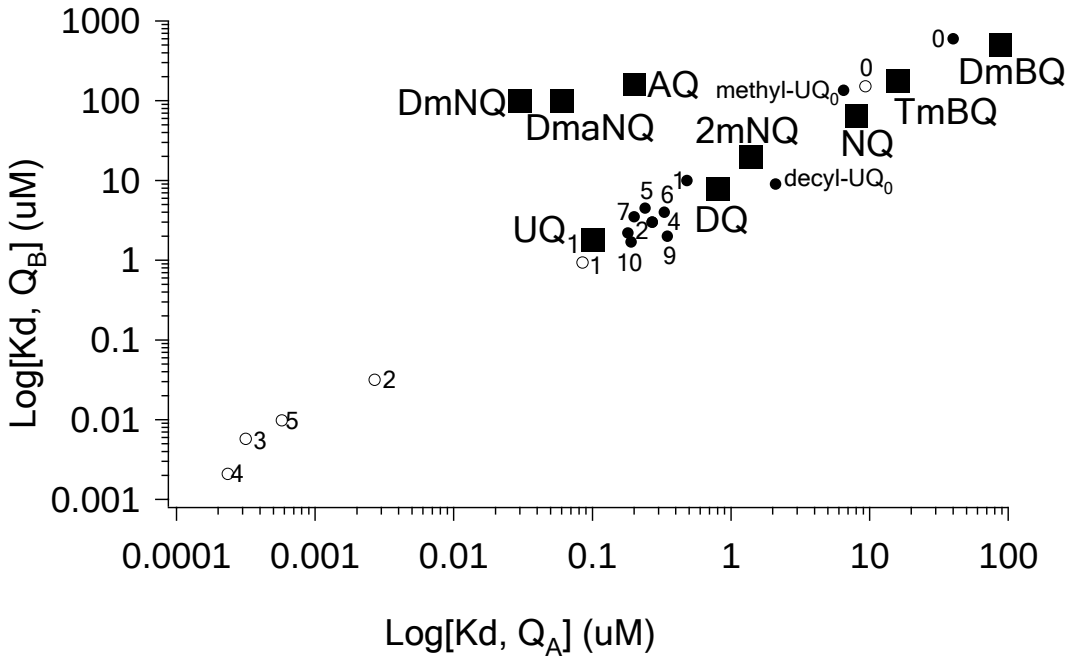

Figure 3.7: Comparison of quinone binding affinity at Q_A and Q_B sites. This work measured in 10mM Tris, pH = 8.0, 0.005% LDAO at 298±2K. Ubiquinone with different tail length in (○): water-saturated hexane (Warncke, Gunner et al. 1994); (●): in 10mM Tris, pH= 8.0, 0.1% LDAO, 298K. The number refers to the number of isopropyl units. Straight line: K_d (Q_A) = K_d (Q_B)/13.

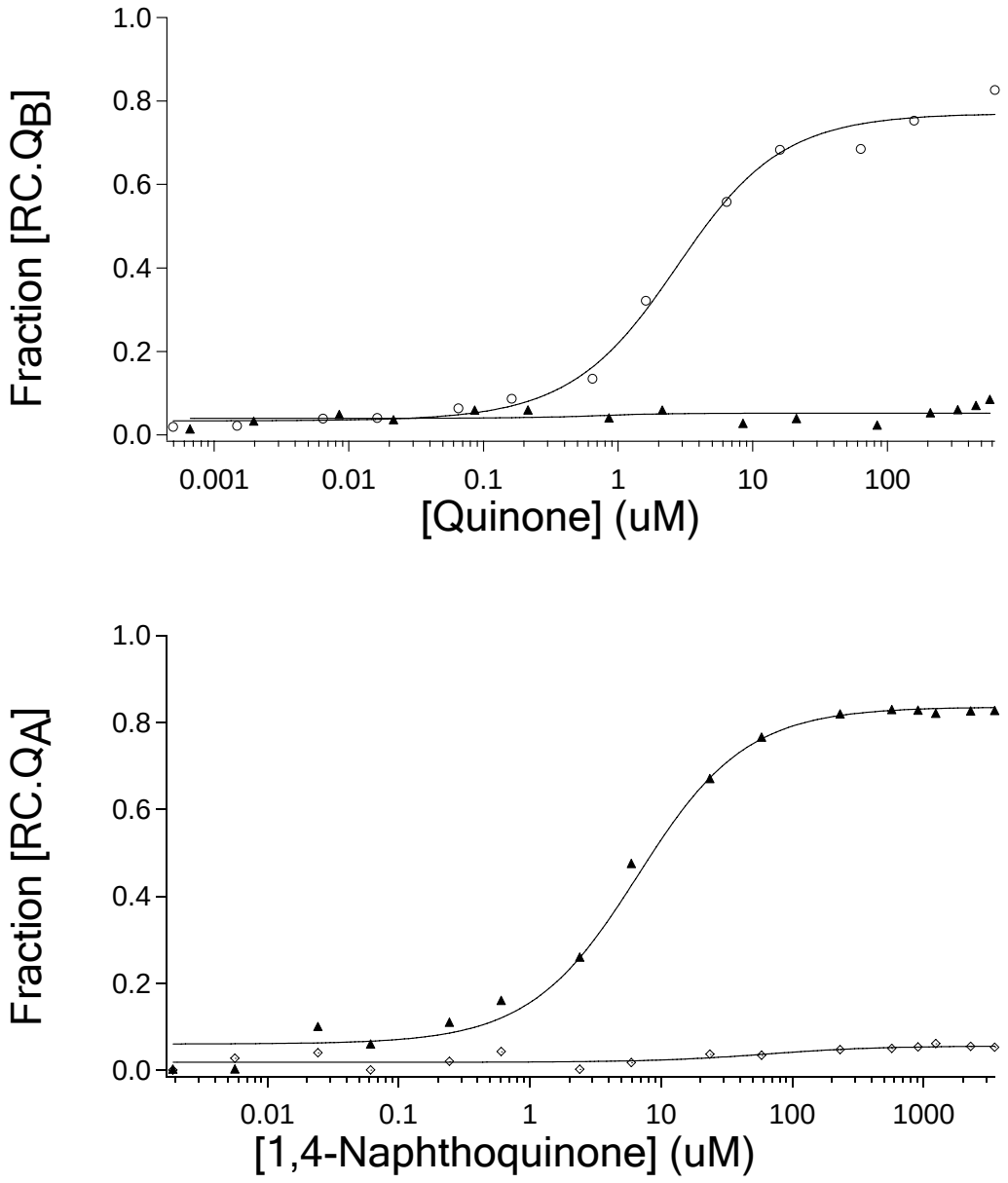

Figure 3.8: a) The binding curve for formation of $P^+Q_B^-$ with UQ_1 at the Q_B site. UQ_1 (○, 10/s), K_d = 1.8 μM at Q_B; NQ (▲, 7.8/s), K_d > 60 μM at Q_B. b) Titration of 1,4-NQ to Q_A-empty RCs. (▲) the fraction of [RC·Q_A] measured with fixed charge recombination rate 7.8/s. (◊) the fraction of [RC·Q_A] which measured with fixed charge recombination rate 0.68/s. This rate is found for electron transfer reaction when NQ is functional at Q_B site with dMA-NQ as Q_A.

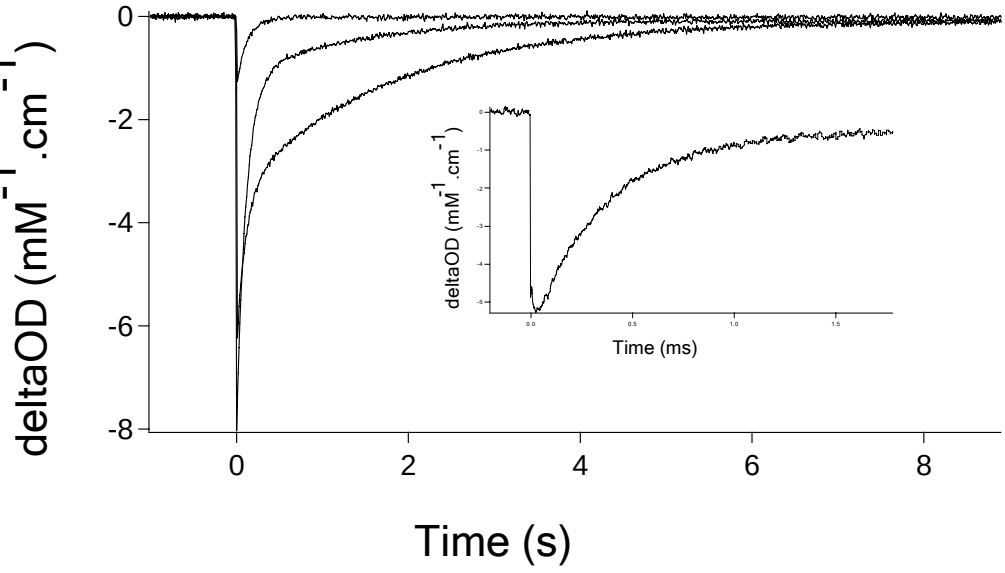

Figure 3.9: Kinetics of charge recombination with different distribution of quinones at each binding site measured at 430 nm following the formation and decay of the P^+ signal. The trace before any quinone addition is subtracted each kinetic trace. The signals have been fitted to the sum of two exponential decays. *Upper trace*: only dMA-NA added to Q_A. *Middle trace:* only NQ added at Q_A: k_1 = 7.8/s, A_1 = 87%; k_2 = 0.68/s, A_2 = 13%. *Lower trace*: dMA-NQ and NQ added. [dMA-NQ] = 2 μM. Phase1: k = 7.8/s, A = 55%; k = 0.68/s, A = 45%. The curve in inset indicates the kinetic trace of dMA-NQ at Q_A at a faster times scale fit to a single exponential: k_1 = 3000/s, A_1 = 95%. 1μM RCs, 0.005% LDAO, 10 mM Tris, pH = 8.0 at room temperature.

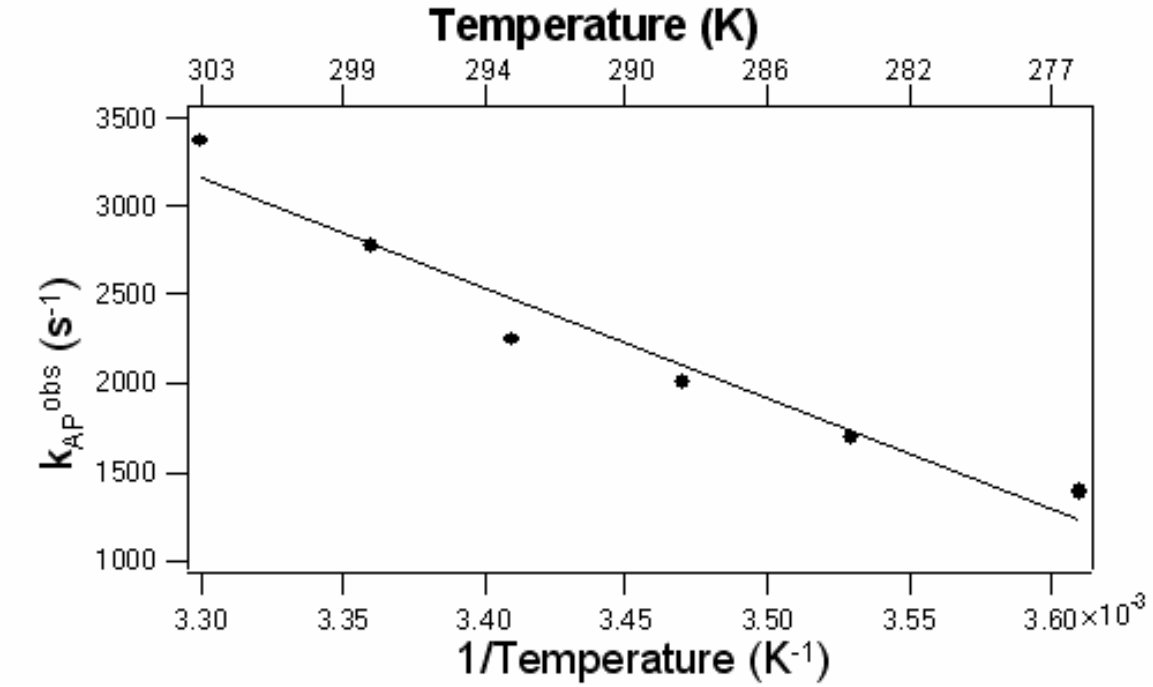

Figure 3.10 Temperature dependence of the $P^+Q_A^-$ charge recombination rate (single exponential fit) with the quinone dMA-NQ at Q_A. ΔH^o is –244 meV and $-T\Delta S^o$ is -19 meV at 298K.

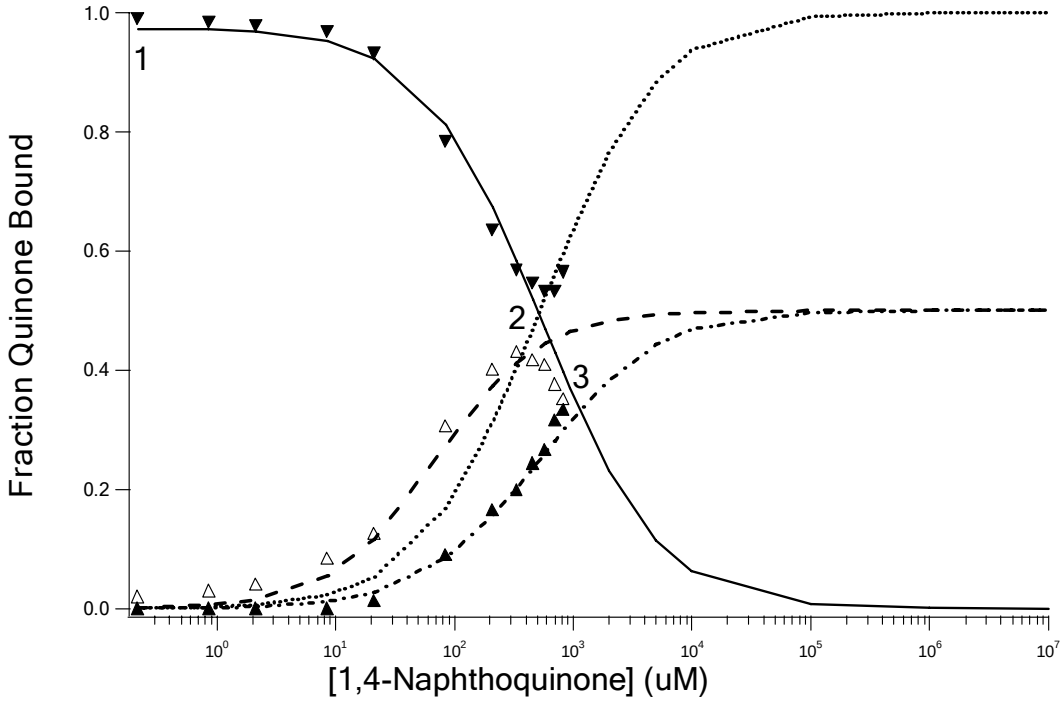

Figure 3.11 Measured fraction of each quinone in each site in RCs with dMA-NQ as XQ at the Q_A site, and NQ as YQ at both Q_A and Q_B sites as a function of the concentration of NQ. Three kinds of Reaction centers: XQ_A, YQ_A and XQ_A-YQ_B. The connect reaction of XQ_A, YQ_A and XQ_A-YQ_B are obtained from three exponential fit with fixed rates: k_1 (XQ_A) = 3000/s, k_2 (YQ_A) = 7.8/s and k_3 (XQ_A-YQ_B) = 0.68/s (The lower kinetic curve in Figure 3.9). (▼): the fraction of dMA-NQ at Q_A site; (△): the fraction of functional NQ bound at Q_B site; (▲): the fraction of NQ bound at Q_A site; Point 1: XQ_A = 100%, YQ_A =0%, XQ_A-YQ_B= 0% Point 2: XQ_A = 45%, YQ_A = 20 %, XQ_A-YQ_B = 45%. Point 3: XQ_A = 30%, YQ_A= 30%, XQ_A-YQ_B = 30%. Theory curves (solid line) generated with Mathematica with these parameters: [RC] = 1μM. [dMA-NQ] = 2 μM. K_d of dMA-NQ at Q_A is 0.06 μM, K_d of NQ at Q_A is 8 μM and K_d of NQ at Q_B is 65 μM. Total concentration of NQ is 200 μM. The theoretical binding curves for XQ_A (solid line) and

YQ_B (dashed line) are matched well with the theoretical simulation. However, the binding curve of NQ at Q_A (dotted line) does not fit with experiment data. The dot-dashed line shows a fit with Φ_{XQ} for NQ at Q_A of 50%.

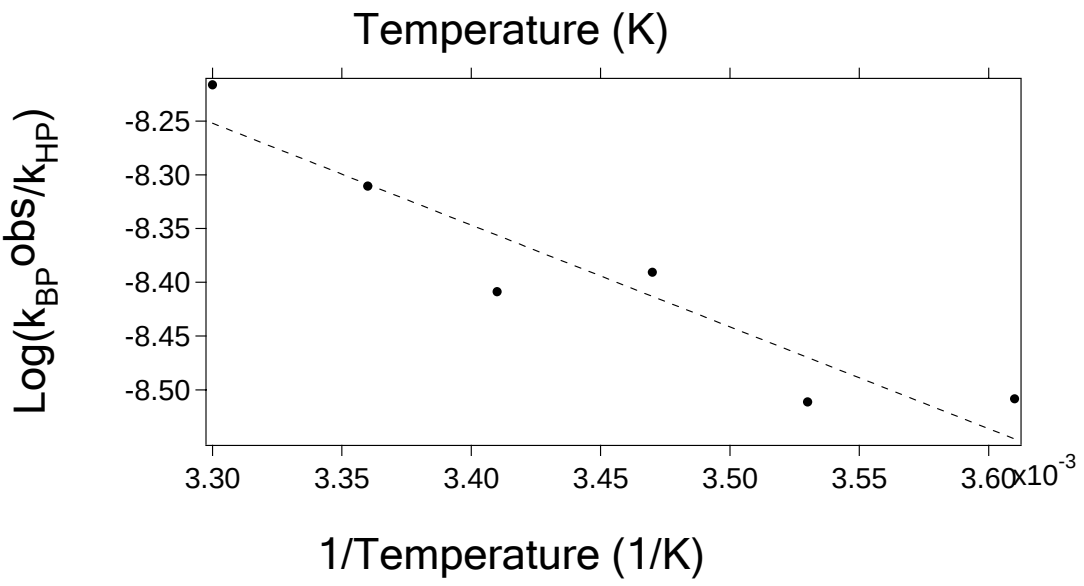

Figure 3.12: Van't Hoff plot for temperature dependence of the $P^{+}Q_B^{-}$ charge recombination rates for reaction centers with dMA-NQ at Q_A and NQ at Q_B. The solid circles represent values measured in the 277K – 303K range. ΔH^o = -188 meV, $-T\Delta S^o$ = -300 meV at 298K.

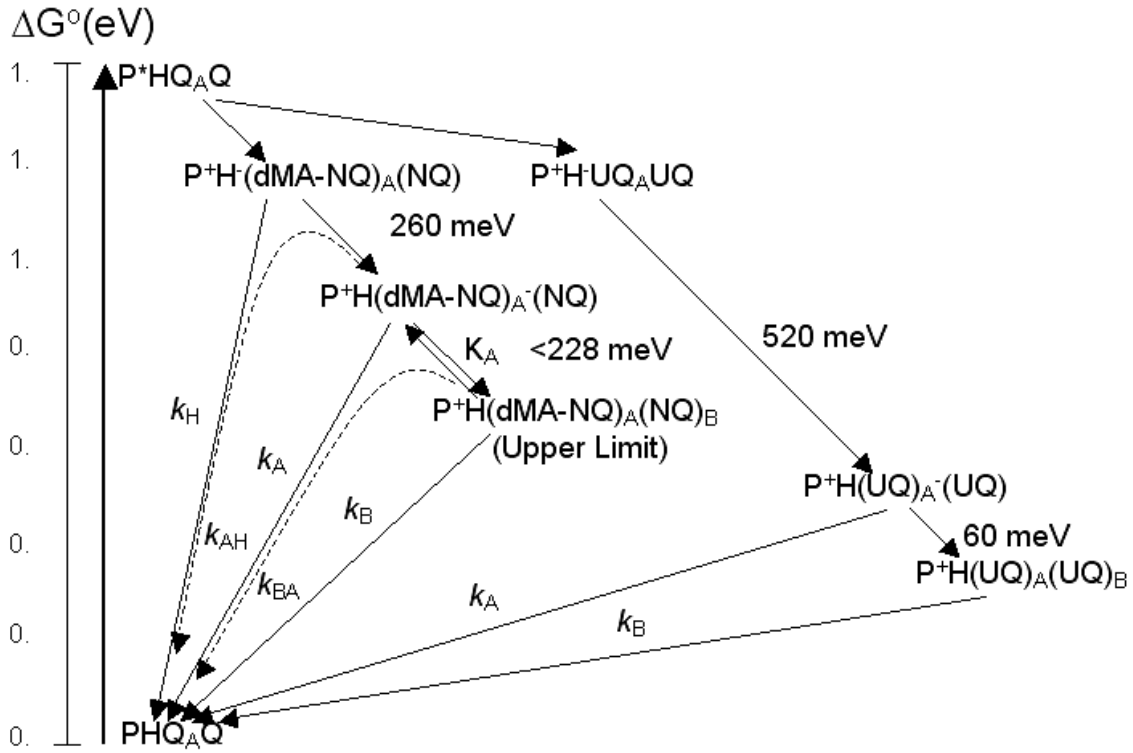

Figure 3.13: The estimated energy levels for NQ and UQ at the Q_A and Q_B sites.

References

Ashnagar, A., Bruce, J. M. et al. (1988) "Synthesis of 2,3-dialkyl-6,7-dichloro- and 2,3-dialkyl-6,7-dibromo-1,4-naphthoquinones." Journal of the Chemical Society, Perkin Transactions 1: Organic and Bio-Organic Chemistry (1972-1999), (3), 559-61

Baccarini-Melandri, A., N. Gabellini, et al. (1980). "Structural requirements of quinone coenzymes for endogenous and dye-mediated coupled electron transport in bacterial photosynthesis." J Bioenerg Biomembr 12(3-4): 95-110.

Cramer, W. A., H. Zhang, et al. (2004). "Evolution of photosynthesis: time-independent structure of the cytochrome b6f complex." Biochemistry 43(20): 5921-9.

Diner, B. A., C. C. Schenck, et al. (1984). "Effect of inhibitors, redox state and isoprenoid chain length on the affinity of ubiquinone for the secondary acceptor binding site in the reaction centers of photosynthetic bacteria." Biochim. Biophys. Acta 766: 9-20.

Fromme, P., P. Jordan, et al. (2001). "Structure of Photosystem I." Biochim. Biophys. Acta 1507: 5-31.

Giangiacomo, K. M. and P. L. Dutton (1989). "In photosynthetic reaction centers, the free energy difference for electron transfer between quinones bound at the primary and secondary quinone-binding sites governs the observed secondary site specificity." Proc. Natl. Acad. Sci. USA 86: 2658-2662.

Gunner, M. R., B. S. Braun, et al. (1985). The characterization of the Q_A binding site of the reaction center of *Rhodopsuedomonas Sphaeroides.* Antenna and Reaction Centers of Photosynthetic Bacteria. M. E. Michel-Beyerle. New York, Springer-Verlag: 298-305.

Gunner, M. R. and P. L. Dutton (1988). Temperature and free energy dependence of the electron transfer to and from Q_A: Electron transfer in reaction center protein from *Rhodobacter Sphaeroides*. The photosynthetic bacterial reaction center: Structure and dynamics. J. Breton and A. Vermeglio. New York, Plenum Press: 259-269.

Gunner, M. R. and P. L. Dutton (1989). "Temperature and $-\Delta G^o$ dependence of the electron transfer from BPh- to Q_A in reaction center protein from *Rhodobacter sphaeroides* with different quinones as Q_A." J. Am. Chem. Soc. 111: 3400-3412.

Gunner, M. R., D. M. Tiede, et al. (1982). Quinones as prosthetic groups in membrane electron-transfer proteins I: Systematic replacement of the primary ubiquinone of photochemical reaction centers with other quinones. Function of Quinones in

Energy Conserving Systems. B. L. Trumpower. New York, Academic Press: 265-269.

Hunte, C., H. Palsdottir, et al. (2003). "Protonmotive pathways and mechanisms in the cytochrome bc1 complex." FEBS Lett 545(1): 39-46.

Kleinfeld, D., M. Y. Okamura, et al. (1984). "Electron transfer in reaction centers of *Rhodopseudomonas sphaeroides:* I. Determination of the charge recombination pathway of $D^+Q_AQ_B^-$ and free energy and kinetic relations between $Q_A^-Q_B$ and $Q_AQ_B^-$." Biochim. Biophys. Acta 766: 126-140.

Kurisu, G., H. Zhang, et al. (2003). "Structure of the cytochrome b6f complex of oxygenic photosynthesis: tuning the cavity." Science 302(5647): 1009-14.

Li, J., D. Gilroy, et al. (1998). "Kinetic phases in the electron transfer from $P^+Q_A^-Q_B$ to $P^+Q_AQ_B^-$ and the associated processes in *Rhodobacter sphaeroides* R-26 reaction centers." Biochemistry 37(9): 2818-2829.

Li, J., E. Takahashi, et al. (2000). "$-\Delta G^o_{AB}$ and pH dependence on the electron transfer from $P^+Q_A^-Q_B$ to $P^+Q_AQ_B^-$ in *Rhodobacter sphaeroides* reaction centers." Biochemistry 39: 7445-7454.

Madeo, J. and M. R. Gunner (2005). "Modeling binding kinetics at the Q_A site in bacterial reaction centers." Biochemistry 44: 10994-11004.

Mancino, L. J., D. P. Dean, et al. (1984). "Kinetics and thermodynamics of the $P870^+Q_A^-$ to $P870^+Q_B^-$ reaction in isolated reaction centers from the photosynthetic bacterium *Rhodopseudomonas sphaeroides."* Biochim. Biophys. Acta 764: 46-54.

Mancino, L. J., D. P. Dean, et al. (1984). "Kinetics and thermodynamics of the $P870^+Q_A^-$ ->$P870^+Q_B^-$ reaction in isolated reaction centers from the photosynthetic bacterium *Rhodopseudomonas sphaeroides."* Biochim. Biophys. Acta 764: 46-54.

Martin, J. L., J. Breton, et al. (1986). "Femtosecond spectroscopy of electron transfer in the reaction center of the photosynthetic bacterium *Rhosopseudomonas sphaeroides* R-26: Direct electron transfer from the dimeric bacteriochlorophys primary donor to the bacteriophoephytin acceptor with a time constant of 2.8+/-0.2 psec." Proc. Natl. Acad. Sci. USA 83: 957-961.

McComb, J. C., R. R. Stein, et al. (1990). "Investigations on the influence of headgroup substitution and isoprene side-chain length in the function of primary and secondary quinones of bacterial reaction centers." Biochim. Biophys. Acta 1015: 156-171.

Okamura, M. Y., R. A. Isaacson, et al. (1975). "The primary acceptor in bacterial photosynthesis: Obligatory role of ubiquinone in photoactive reaction centers of *Rhodopseudomonas sphaeroides." P*roc. Natl. Acad. Sci. USA 72: 3492-3496.

Okamura, M. Y., M. L. Paddock, et al. (2000). "Proton and electron transfer in bacterial reaction centers." Biochim. Biophys. Acta 1458: 148-163.

Rutherford, A. W. and A. Krieger-Liszkay (2001). "Herbicide-induced oxidative stress in photosystem II." Trends Biochem Sci. 26: 648-653.

Salmon-Chemin, L., E. Buisine, et al. (2001). "2- and 3-substituted 1,4-naphthoquinone derivatives as subversive substrates of trypanothione reductase and lipoamide dehydrogenate from Typan*osoma cruzi: Syn*thesis and correlation between redox cycling activities and in vitro cytotoxicity." J. Med. Chem. 44: 548-565.

Schmid, R. and A. Labahn (2000). "Temperature and free energy dependence of the direct charge recombination rate from the secondary quinone in bacteria reaction centers from *Rhodobacter sphaeroides." J.* Phys. Chem. B. 104(13): 2928-2936.

Shopes, R. J. and C. A. Wraight (1987). "Charge recombination from the $P^+Q_A^-$ state in reaction centers from *Rhodopseudomonas viridis." Bi*ochim. Biophys. Acta 893: 409-425.

Stowell, M. H. B., T. M. McPhillips, et al. (1997). " Light-induced structural changes in photosynthetic reaction center: implications for mechanism of electron-proton transfer." Science 276: 812-816.

Stroebel, D., Y. Choquet, et al. (2003). "An atypical haem in the cytochrome b(6)f complex." Nature 426(6965): 413-8.

Tiede, D. M., J. Vazquez, et al. (1996). "Time-resolved electrochromism associated with the formation of quinone anions in the Rhodo*bacter sphaeroides R-26* reaction center." Biochemistry 35: 10763-10775.

Warncke, K. and P. L. Dutton (1993). "Influence of Q_A site redox cofactor structure on equilibrium binding, in situ electrochemistry, and electron-transfer performance in the photosynthetic reaction center protein." Biochemistry 32(18): 4769-79.

Warncke, K., M. R. Gunner, et al. (1994). "Influence of hydrocarbon tail structure on quinone binding and electron-transfer performance at the Q_A and Q_B sites of the photosynthetic reaction center protein." Biochemistry 33: 7830-7841.

Warncke, K., M. R. Gunner, et al. (1987). Effect of hydrocarbon tail structure on the affinity of substituted quinones for the Q_A site in reaction centers of

Rhodoppseudomonas sphaeroides R-26. Progress in Photosynthesis Rearch. J. Biggins. Dordrecht, Martinus Nijhoff. i: 217-220.

Woodbury, N. W., M. Becker, et al. (1985). "Picosecond kinetics of the initial photochemical electron-transfer reaction in bacterial photosynthetic reaction centers." Biochemistry 24: 7516-7521.

Woodbury, N. W., W. W. Parson, et al. (1986). "Radical-pair energetics and decay mechanisms in reaction center containing anthraquinones or benzoquinones in place of ubiquinone." Biochim. Biophys. Acta. 851: 6-22.

Wraight, C. A. (1979). "The role of quinones in bacterial photosynthesis." Photochem. Photobiol. 30: 767-776.

Xu, Q. and M. R. Gunner (2000). "Temperature dependence of the free energy, enthalpy and entropy of $P^{+}Q_{A-}$ charge recombination in photosynthetic reaction centers." J.Phys.Chem. B 104: 8035-8043.

Zhu, Z. and M. R. Gunner (2005). "Energetics of quinone-dependent electron and proton transfers in *Rhodobacter sphaeroides* photosynthetic reaction centers." Biochemistry 44: 82-96.